




Effects of Ni(P) layer thickness and Pd layer type in thin-Au/Pd/Ni(P) surface finishes on interfacial reactions and mechanical strength of Sn–58Bi solder joints during aging

Jungsoo Kim¹, Seung-Boo Jung^{2,*}, and Jeong-Won Yoon^{3,*} 

¹Advanced Functional Material R&D Department, Korea Institute of Industrial Technology (KITECH), 156 Gaetbeol-ro, Yeonsu-gu, Incheon 21999, Korea

²School of Advanced Materials Science & Engineering, Sungkyunkwan University, 2066 Seobu-ro, Jangan-gu, Suwon 16419, Gyeonggi-do, Korea

³Department of Advanced Materials Engineering, Chungbuk National University, 1 Chungdae-ro, Seowon-gu, Cheongju 28644, Chungbuk, Korea

Received: 10 August 2020

Accepted: 16 September 2020

Published online:

27 September 2020

© Springer Science+Business Media, LLC, part of Springer Nature 2020

ABSTRACT

To analyze the effects of Ni(P) layer thickness and Pd layer composition on interfacial reactions and the mechanical reliabilities of Sn–58Bi solder joints, we evaluated a phosphorous-contained Ni (Ni(P)) layer thicknesses ranging from 0.3 to 1.0 μm with Au/Pd/Ni(P) or a phosphorous-contained Pd [Au/Pd(P)/Ni(P)] layer in thin-electroless-nickel electroless-palladium immersion gold (ENEPIG) with Sn–58Bi solder joint after aging test. (Pd, Au) Sn_4 and Ni_3Sn_4 intermetallic compounds (IMCs) were dominantly formed at the interfaces of the 0.3 μm to 1.0 μm Ni(P) layers in the thin-Au/Pd/Ni(P) or thin-Au/Pd(P)/Ni(P) joints after aging at 85 $^\circ\text{C}$ and 95 $^\circ\text{C}$ for 100 h. However, the Ni_3Sn_4 IMC layer changed to the (Cu, Ni) $_6\text{Sn}_5$ IMC layer in the 0.3 μm Ni(P) layer contained the Au/Pd/Ni(P) joint after aging at 85 $^\circ\text{C}$ for 300 h, because the Cu elements in a Cu pad penetrated through the P-rich Ni layer. Otherwise, the Ni_3Sn_4 IMC of the 0.3 μm Ni(P) layer in the Au/Pd(P)/Ni(P) joint changed to (Ni, Cu) $_3\text{Sn}_4$ IMC after aging at 105 $^\circ\text{C}$ and 115 $^\circ\text{C}$ for 1000 h, due to the P in the Pd layer, which affects the IMC growth rate. The 0.7 μm and 1.0 μm Ni(P) layers in the Au/Pd/Ni(P) or Au/Pd(P)/Ni(P) joints were attributed to the Ni_3Sn_4 IMC layer for whole aging conditions because the thick P-rich Ni layer suppress Sn and Cu diffusion during aging. In a high-speed shear tests, the shear strength of the 0.3 μm Ni(P) layer in the Au/Pd/Ni(P) joints was relatively low than that of the Au/Pd(P)/Ni(P) joints after aging at 105 $^\circ\text{C}$ and 115 $^\circ\text{C}$ for 100 h. Ni_3Sn_4 IMC was observed at the fracture surfaces of the 0.3 μm Ni(P) layer in the Au/Pd(P)/Ni(P) joints after aging at 115 $^\circ\text{C}$ for 1000 h, whereas the fracture surface of the

Address correspondence to E-mail: sbjung@skku.edu; jwyoonyoon@chungbuk.ac.kr

Au/Pd/Ni(P) joint was Cu substrate. Therefore, Ni(P) layer thicknesses in excess of 0.7 μm and the P-containing Pd layer in the thin-ENEPIG surface finish with Sn–58Bi solder joints are expected to be highly reliable after long-term aging treatment.

1 Introduction

Recent 2010s, the trends in electronic packaging technologies have evolved to include high-performance, multi-functionality, large input/output (I/O) density, high-capability, and 3-D integration with downsizing packages [1–4]. In addition, these performances should ensure high mechanical and electrical reliabilities. To achieve these performance requirements, the selection of the solder alloy is one of the most critical factors of reliable interconnection between electronic components and substrates [5]. Not only composition of solder alloy, but also the metallization layer selection is an important aspect of joint reliability under harsh conditions to improve and ensure reliability. The microstructure and intermetallic compounds (IMCs) composition at the interface of solder joint significantly affects joint characteristic and reliability [6, 7]. In general, an excessive Cu–Sn IMCs can form between a bare Cu substrate and Sn-based solder alloys after reflows or aging treatment because of high diffusion rate of Cu (diffusion coefficient of Cu towards Sn, $2.5 \times 10^{-7} \text{ cm}^2/\text{s}$ at 160 °C) [8–10]. To reduce the IMC growth rate and improve joint reliabilities, various surface finishes have been developed as organic solderability preservative (OSP), immersion Sn, immersion Ag, electroless-nickel immersion gold (ENIG), and electroless-nickel electroless-palladium immersion gold (ENEPIG) [10–15]. Among these surface finishes including metallization layers, an ENIG has been widely used over the past few years because of the excellent characteristics of the Ni layer suppress rapid reaction of Cu and Sn elements in each Cu substrate and the Sn-based solder [8, 16–18]. The diffusion coefficient of Ni towards Sn is $5.4 \times 10^{-9} \text{ cm}^2/\text{s}$ is slower than that of Cu [19]. However, the Ni layer can give rise to galvanic hyper-corrosion during the Au layer plating process, called the ‘black pad’ phenomenon [20]. The ‘black pad’ phenomenon results in significantly degraded wettability and joint reliabilities [20–23].

To improve the characteristics of the ENIG, the ENEPIG surface finish which including a Pd layer plating between Ni(P) and Au layer has been developed for the past few years. The Pd layer that is plated on the Ni(P) layer plays an prime role of determining the joint characteristics by acting as a diffusion barrier at the interface between the Cu substrate and the solder, with a Ni(P) layer and a wetting layer with an Au layer [24, 25]. However, a thick Ni(P) layer in the ENEPIG surface finish rapidly increases the electrical resistance of the package interconnection and induces gradual electrical noise that degrades the overall reliability, especially in high-frequency applications [19]. Furthermore, a relatively thick Ni(P) layer with the ENEPIG surface finish compared to other metallization layers has several disadvantages including the difficulty of application to fine-pitch manufacturing and high-cost problems.

To solve these problems associated with the ENEPIG surface finish, an ultra-thin Ni(P) layer thickness (less than 0.5 μm) in the ENEPIG surface finish has been investigated to improve the electrical characteristics and reliabilities of a normal [average 4 μm to 6 μm thickness of Ni(P)] ENEPIG surface finish [26]. However, a few investigators have reported that less than 0.1 μm thickness Ni(P) layer in ultra-thin-ENEPIG with a Sn–3.0Ag–0.5Cu (SAC305) solder joint has a lower electrical impedance compared to a normal Ni(P) layer thickness (4–6 μm) in the ENEPIG with the SAC305 solder joint [19, 27]. Yoon reported that the shear strength of solder joint with a less than 0.3 μm thick Ni(P) layer is similar to that of normal ENEPIG with reflow times of 180 s [28]. Although several studies on thin-ENEPIG surface finishes with Sn-based solder joints have been performed, there are limited reports on thin-ENEPIG surface finish with low melting temperatures of Sn-based solder, especially Sn–Bi solder joints with aging treatment.

Therefore, we investigated two kinds of Pd layers as the pure Pd [Au/Pd/Ni(P)] and phosphorous-containing Pd [Au/Pd(P)/Ni(P)] with different Ni(P) thickness contained the thin-ENEPIG surface

finishes with a Sn–58Bi solder joint after aging treatment. Thermal and mechanical stresses were inter-related in the joint because different coefficient of thermal expansion (CTE) value between the substrate and solder can occur at mechanical fracture as cracks propagate through the interface of solder joints [29, 30]. Therefore, we investigated different Ni(P) layers thicknesses as a range of 0.3 μm to 1.0 μm with Au/Pd/Ni(P) or Au/Pd(P)/Ni(P) surface finish with Sn–58Bi solder joints under various aging conditions.

2 Experimental

In this research, different Ni(P) layer thicknesses in a range of 0.3 μm to 1.0 μm [denoted as 0.3 to 1.0 μm Ni(P)] with Au/Pd/Ni(P) or Au/Pd(P)/Ni(P) layer contained in thin-ENEPIG PCBs with Sn–58Bi solder joints (hereafter referred to as a Au/Pd/Ni(P) joint or Au/Pd(P)/Ni(P) joint) under different aging times and temperatures were investigated. A schematic diagram of two types of the ENEPIG surface-finished PCB substrates is featured in Fig. 1. The thin-ENEPIG surface finishes were composed of 0.3, 0.5, 0.7, and 1.0 μm thicknesses of Ni(P) layers with 0.1 μm thickness of each Au/Pd/Ni(P) or Au/Pd(P)/Ni(P) and 0.1 μm thickness of Au layers, plated on a Cu substrate. Reducing agents such as formic acid and hypophosphoric acid are used to form the Au/Pd/Ni(P) and Au/Pd(P)/Ni(P) layers, respectively. The Sn–58Bi solder paste (TLF-401-11; Tamura Co., Japan) was printed on the 350 μm diameter of the ENEPIG-plated Cu pad in the PCB using screen-printing method. Next, 450 μm diameter Sn–58Bi solder balls (Duksan Hi-Metal Co., Ltd., Korea) were placed on the printed Sn–58Bi solder paste and a reflow was conducted for 400 s with a peak temperature of 190 $^{\circ}\text{C}$ by using a reflow machine (Heller Co., Ltd., USA). Figure 2a shows the reflow temperature profile. After the reflow process, fluxes in a samples were eliminated using de-flux solution. The

aging treatments were performed at different temperatures of each 85, 95, 105, and 115 $^{\circ}\text{C}$ for 100 to 1000 h. The aging condition was based on the Joint Electron Device and Engineering Council (JEDEC) JESD-47 standard. The low- and high-speed shear strengths of the Sn–58Bi/thin-ENEPIG joints were conducted and evaluated after aging treatment by using global bond testers (DAGE-4000HS and DAGE-4000, Nordson, DAGE, UK). The high- and low-speed shear conditions were 1 m/s and 200 $\mu\text{m}/\text{s}$ shear speed at a shear height of approximately 50 μm , respectively. The shear conditions were based on the JEDEC standard 22-B117A. Schematic diagrams of the high- and low-speed shear tests and conditions are shown in Fig. 2b.

The microstructures and IMC morphologies of the Sn–58Bi/thin-ENEPIG solder joints were analyzed by using scanning electron microscopy (SEM, INSPECT, F, FEI, USA) and field-emission transmission electron microscopy (FE-TEM, JEM-F200, JEOL Ltd., Japan). The IMCs composition and the fracture surfaces after high- and low-speed shear tests of the Sn–58Bi/thin-ENEPIG solder joints were defined by using energy-dispersive x-ray spectroscopy (EDS). We investigated the microstructure behavior and mechanical strength of Sn–58Bi/thin-ENEPIG joints with. The results [31] are used here only to provide a direct comparison of the Ni(P) layer thickness which affects the interfacial reaction and the mechanical reliabilities of thin-ENEPIG surface-finished PCB with Sn–58Bi solder joints under aging.

3 Results and discussion

3.1 Microstructure evolution during aging

Figure 3 shows cross-sectional SEM micrographs of 0.3 μm to 1.0 μm Ni(P)–Au/Pd/Ni(P) joints after reflow. Flake- and layer-type (Pd, Au)Sn₄ IMC were formed at the interface between the Sn–Bi alloy and Ni(P) layer of the joints. Bi-rich (white-gray color)

Fig. 1 Schematic diagrams of **a** normal ENEPIG and **b** thin-ENEPIG surface-finished PCB substrates (Color figure online)

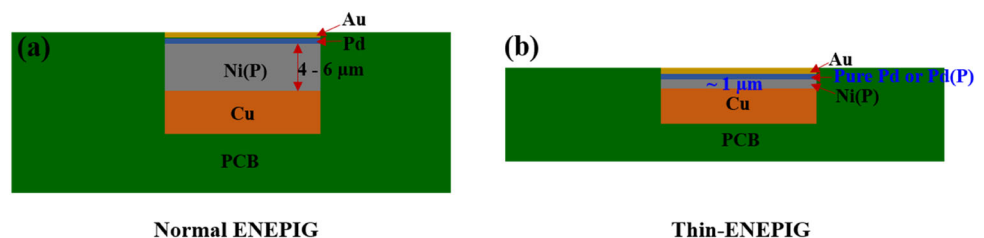


Fig. 2 **a** Reflow temperature profile and **b** schematic diagram of low- and high-speed shear testing conditions (Color figure online)

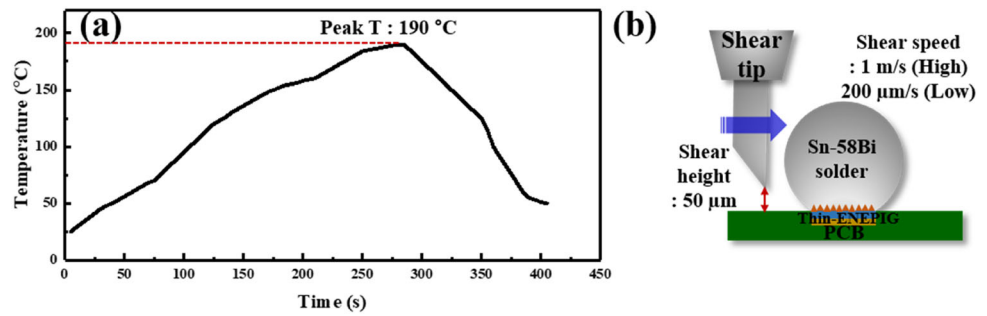
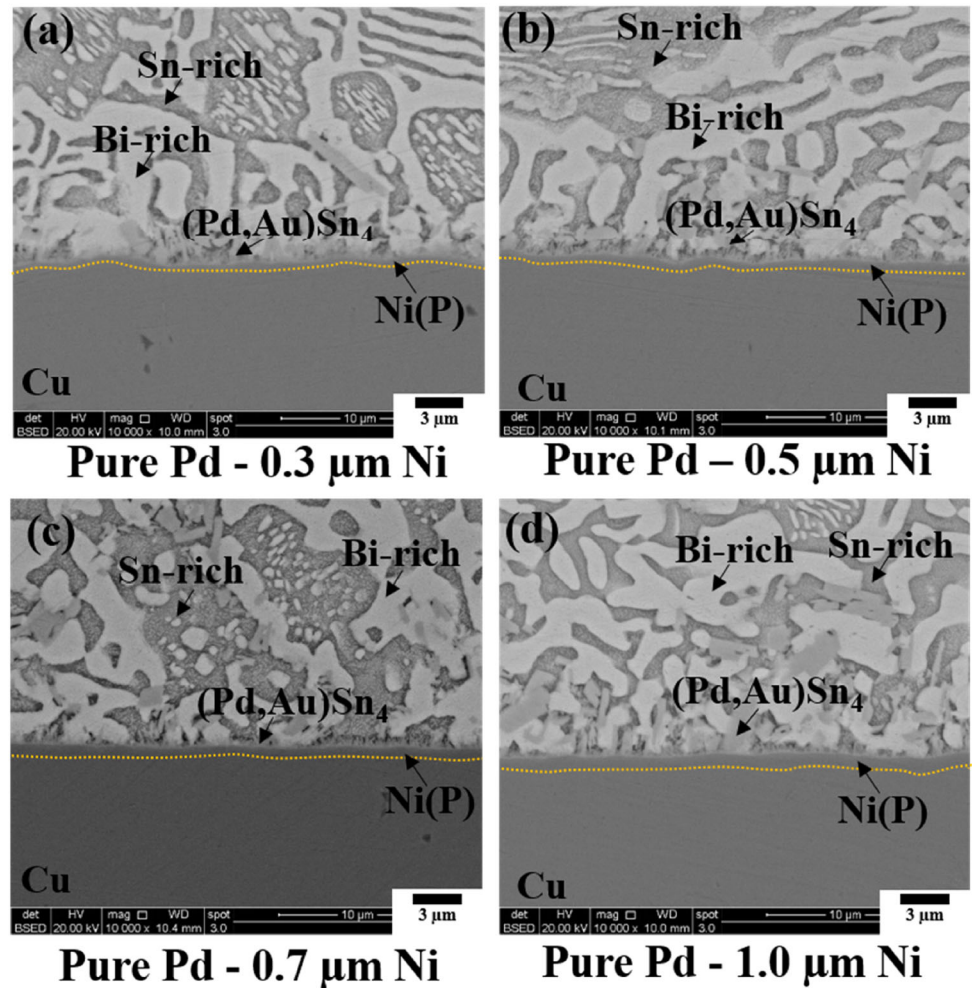


Fig. 3 Cross-sectional SEM micrographs of various Ni(P) layer thickness with Au/Pd/Ni(P) layer in thin-ENEPIG surface-finished PCB with Sn–58Bi solder joints after reflow: **a** 0.3 μm Ni(P), **b** 0.5 μm Ni(P), **c** 0.7 μm Ni(P), and **d** 1.0 μm Ni(P) (Color figure online)



and Sn-rich (dark-gray color) regions were observed with parallel lamellar structures in the Sn–Bi alloy. This is reason that the Sn elements have similar volume percentages with Bi elements. The interfaces between Cu substrate and the Ni(P) layer are represented using yellow lines as shown in Fig. 3. The Au and Pd layers in the ENEPIG were sequentially reacted with Sn elements in the Sn–Bi solder alloy. As a result, the formation of the (Pd, Au)Sn₄ interface

was formed at the interface during reflow. In general, the Au and Pd metallization layers between Sn–Bi solder and Ni(P) layer are affected by relatively low thermal energies than that of Sn–Ag–Cu solder alloys during reflow and aging. In addition, Bi in the Sn–Bi solder alloy blocks Au and Pd elements dissolved from each metallization layer region to Sn–Bi solder. For these reasons, the Pd and Au elements are not dissolved into the Sn–Bi solder after reflow, and

mostly forming IMC with Sn in the Sn–Bi solder. However, Ni elements in the Ni(P) layer did not participate to form IMCs with Sn and existed as plating Ni(P) in its initial state until the (Pd, Au)Sn₄ IMC-forming period. For this reason, no significant differences in microstructural evolution occurred at the interfaces of the solder joints with various Ni layer thicknesses, as shown in Fig. 3.

To analyze the effects of the different Ni(P) layer thickness in the Au/Pd/Ni(P) joints on the microstructure behavior during aging treatment, various aging conditions were performed for different temperatures and times. Figure 4 shows cross-

sectional SEM micrographs of the 0.3 μm to 1.0 μm Ni(P)–Au/Pd/Ni(P) joints after aging at 85 °C for up to 1000 h. The (Pd, Au)Sn₄ and Ni₃Sn₄ IMCs were dominantly formed at the interface between the P-rich Ni layer and Sn–Bi alloy of all Ni(P)–Au/Pd/Ni(P) joints after aging for 100 h. However, the Ni₃Sn₄ IMC layer composition was changed to (Cu, Ni)₆Sn₅ IMC, which was formed between the (Pd, Au)Sn₄ IMC layer and the P-rich Ni layer of the 0.3 μm Ni(P)–Au/Pd/Ni(P) joints after aging for 300 h. In addition, part of the P-rich Ni layer was destroyed after aging for 500 h. The white arrow in the figure indicates the destroyed part of the P-rich

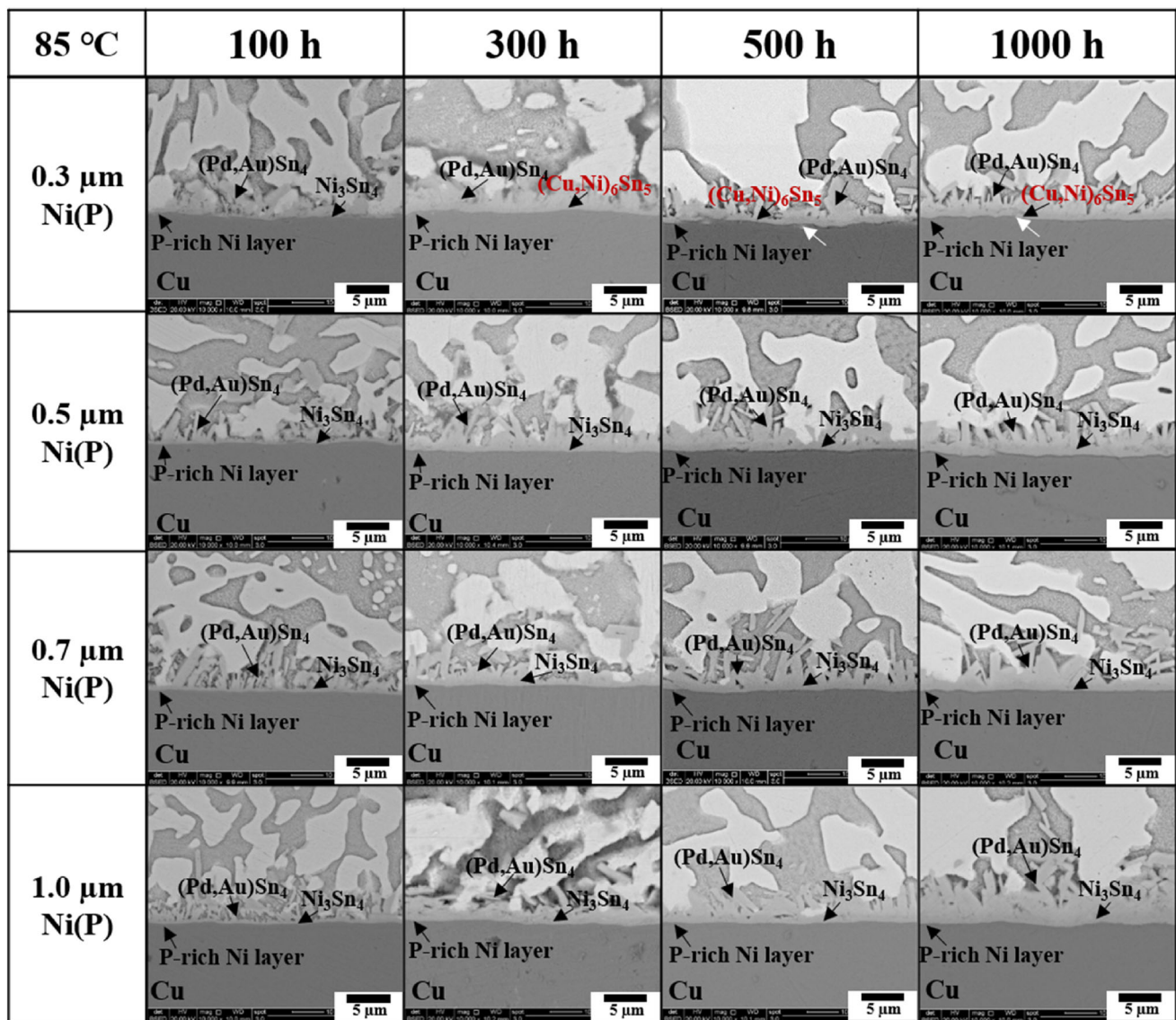


Fig. 4 Cross-sectional SEM micrographs of various Ni(P) layer thickness with Au/Pd/Ni(P) layer contained thin-ENEPIG surface-finished PCB with Sn–58Bi solder joints after aging at 85 °C (Color figure online)

Ni layer. The P-rich Ni layer of the 0.3 μm Ni(P)–Au/Pd/Ni(P) joints was mostly consumed, and the Cu in the underlying Cu substrate participated in the interfacial reaction. For these reasons, IMC composition of the 0.3 μm Ni(P)–Au/Pd/Ni(P) joint was $(\text{Cu}, \text{Ni})_6\text{Sn}_5$. In contrast, the Ni_3Sn_4 IMC layers were still positioned and coarsened at the interface of the 0.5 μm to 1.0 μm Ni(P)–Au/Pd/Ni(P) joints after aging for 1000 h due to the Ni(P) plating layers and the formed P-rich Ni layers of the 0.5 μm to 1.0 μm Ni(P)–Au/Pd/Ni(P) joints were thicker than that of the 0.3 μm Ni(P)–Au/Pd/Ni(P) joint. Therefore, the P-rich Ni layers at the interfaces remained intact and the Ni in the remaining Ni(P) layers are sufficient to diffuse and grow, forming a Ni_3Sn_4 IMC layer with Sn in the Sn–Bi alloy during aging at 85 $^\circ\text{C}$ for 1000 h.

Figure 5 shows cross-sectional SEM micrographs of the 0.3 μm to 1.0 μm Ni(P)–Au/Pd/Ni(P) joints after aging at 95 $^\circ\text{C}$ for 1000 h. The $(\text{Pd}, \text{Au})\text{Sn}_4$ and Ni_3Sn_4 IMCs of all the Ni(P) layers in the Au/Pd/Ni(P) joints after aging at 95 $^\circ\text{C}$ were slightly coarsened compared to those obtained after aging at 85 $^\circ\text{C}$. The Ni_3Sn_4 IMC layer of the 0.3 μm Ni(P)–Au/Pd/Ni(P) joint was changed to the $(\text{Cu}, \text{Ni})_6\text{Sn}_5$ IMC after aging at 95 $^\circ\text{C}$ for 300 h and part of the P-rich Ni layer was destroyed after aging for 500 h. Although the aging temperature increased from 85 to 95 $^\circ\text{C}$, the Ni_3Sn_4 IMC layers of the 0.5 μm to 1.0 μm Ni(P)–Au/Pd/Ni(P) joints remained at the interface between $(\text{Pd}, \text{Au})\text{Sn}_4$ IMC and the P-rich Ni layer after aging for 1000 h, and observed similar morphologies compared to those obtained after aging at 85 $^\circ\text{C}$.

Figure 6 shows cross-sectional SEM micrographs of the 0.3 μm to 1.0 μm Ni(P)–Au/Pd/Ni(P) joints after aging at 105 $^\circ\text{C}$ for 1000 h. The $(\text{Cu}, \text{Ni})_6\text{Sn}_5$ IMC was dominantly formed at the interface of the 0.3 μm Ni(P)–Au/Pd/Ni(P) joints after aging for 100 h. In addition, part of the P-rich Ni layer was destroyed after aging for 300 h. In the case of the 0.5 μm Ni(P)–Au/Pd/Ni(P) joints, the Ni_3Sn_4 IMC was changed to $(\text{Ni}, \text{Cu})_3\text{Sn}_4$ IMC after aging for 500 h. This is because the Ni in the Ni(P) layer was almost completely consumed to form Ni_3Sn_4 IMC before changing to $(\text{Ni}, \text{Cu})_3\text{Sn}_4$ IMC. Sequentially, the Cu element in the underlying Cu layer participated in the interfacial reactions. However, the 0.7 and 1.0 μm Ni(P)–Au/Pd/Ni(P) joints were still composed of the $(\text{Pd}, \text{Au})\text{Sn}_4$ and Ni_3Sn_4 IMCs after aging for 1000 h.

Figure 7 shows cross-sectional SEM micrographs of the 0.3 μm to 1.0 μm Ni(P)–Au/Pd/Ni(P) joints

after aging at 115 $^\circ\text{C}$ for 1000 h. The IMC compositions of these joints after aging at 115 $^\circ\text{C}$ were similar to those obtained after aging at 105 $^\circ\text{C}$, because the Ni in the Ni(P) layer was completely consumed and part of the P-rich Ni layer was destroyed after aging at 105 $^\circ\text{C}$. In contrast, the $(\text{Pd}, \text{Au})\text{Sn}_4$ and Ni_3Sn_4 IMCs of the 0.7 μm and 1.0 μm Ni(P)–Au/Pd/Ni(P) joints did not change and gradually became coarse with the increase in the aging time up to 115 $^\circ\text{C}$ for 1000 h. The P-rich Ni layers of the 0.7 μm and 1.0 μm Ni(P)–Au/Pd/Ni(P) joints were hold up to after aging at 115 $^\circ\text{C}$ for 1000 h.

Figure 8 shows cross-sectional SEM micrographs of the 0.3 μm to 1.0 μm Ni(P)–Au/Pd(P)/Ni(P) joint after reflows. Unlike the flake- and layer-type $(\text{Pd}, \text{Au})\text{Sn}_4$ IMCs formed at the interface of the Au/Pd/Ni(P) joint after reflows (Fig. 3), most of the flake-type $(\text{Pd}, \text{Au})\text{Sn}_4$ IMC was detached at the interface of the Au/Pd(P)/Ni(P) joint and spalled toward the Sn–Bi solder alloy.

Figure 9 shows cross-sectional SEM micrographs of the 0.3 μm to 1.0 μm Ni(P)–Au/Pd(P)/Ni(P) joints after aging at 85 $^\circ\text{C}$ for 1000 h. Partially remained flake-type $(\text{Pd}, \text{Au})\text{Sn}_4$ IMCs were formed at the interface of the Au/Pd(P)/Ni(P) joint after aging for 100 h. After aging for 300 h, layer-type Ni_3Sn_4 IMCs were formed at the interfaces between the $(\text{Pd}, \text{Au})\text{Sn}_4$ IMC and P-rich Ni layer of the 0.3 μm to 1.0 μm Ni(P)–Au/Pd(P)/Ni(P) joints. Under the same conditions as aging at 85 $^\circ\text{C}$ for 100 h, differences in the IMC composition and morphology were observed in the Au/Pd(P)/Ni(P) and Au/Pd/Ni(P) joints. The $(\text{Pd}, \text{Au})\text{Sn}_4$ and Ni_3Sn_4 IMCs at the interfaces of all Ni(P)–Au/Pd(P)/Ni(P) joints were slightly coarsened with increased aging up to 1000 h, regardless of Ni(P) layer thickness. The Ni_3Sn_4 IMC and P-rich Ni layer of the 0.3 μm Ni(P)–Au/Pd(P)/Ni(P) joint was completely intact after aging for 1000 h.

Figure 10 shows cross-sectional SEM micrographs of the 0.3 μm to 1.0 μm Ni(P)–Au/Pd(P)/Ni(P) joints after aging at 95 $^\circ\text{C}$ for 1000 h. Ni_3Sn_4 IMC layers were dominantly formed at the interface between the flake-type $(\text{Pd}, \text{Au})\text{Sn}_4$ IMC and the P-rich Ni layer for all Ni(P)–Au/Pd(P)/Ni(P) joints after aging from 100 to 1000 h. The $(\text{Pd}, \text{Au})\text{Sn}_4$ and Ni_3Sn_4 IMCs of Au/Pd(P)/Ni(P) joints were slightly coarsened after aging at 95 $^\circ\text{C}$ compared to those aged at 85 $^\circ\text{C}$.

Figure 11 shows cross-sectional SEM micrographs of the 0.3 μm to 1.0 μm Ni(P)–Au/Pd(P)/Ni(P) joints

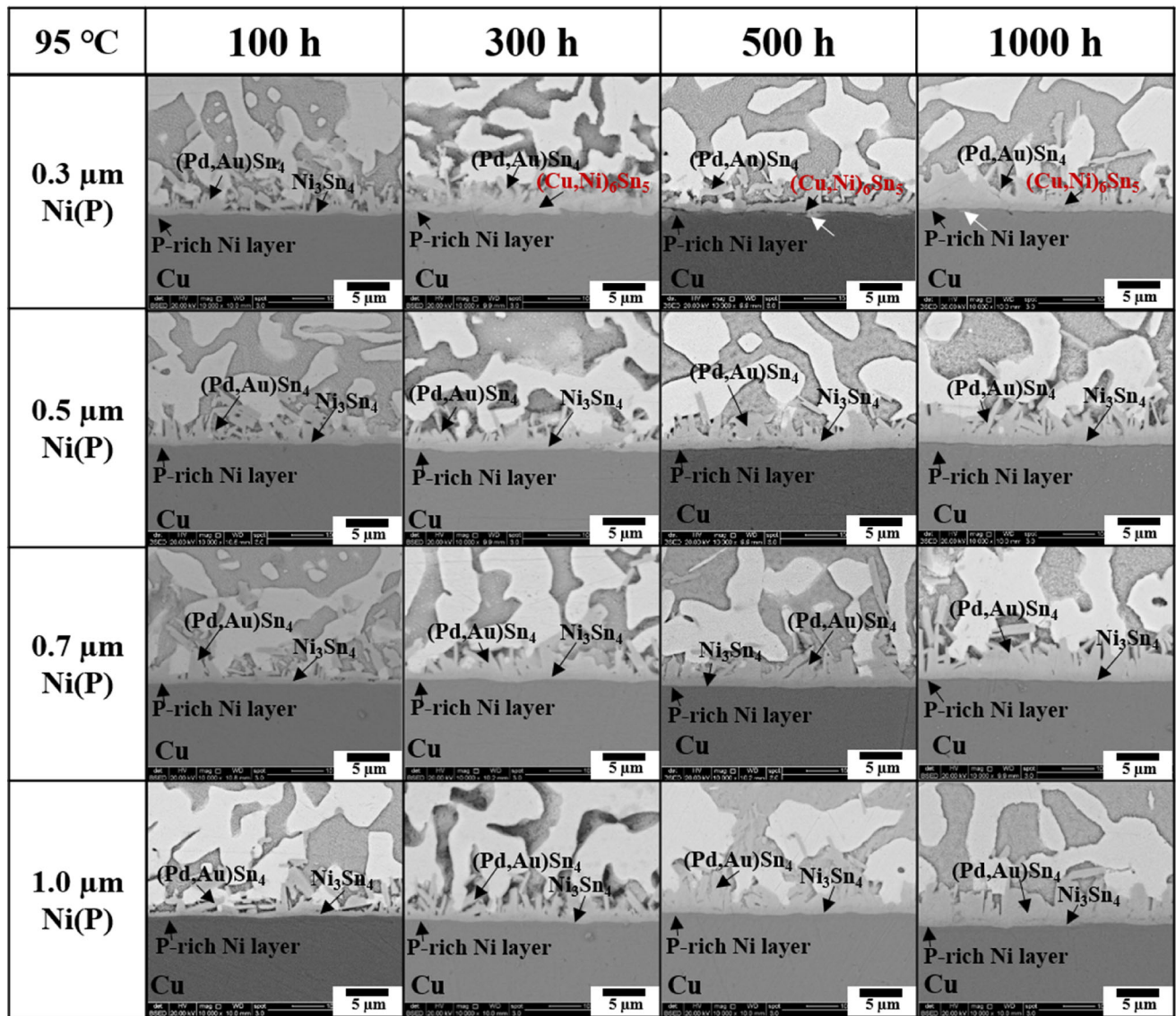


Fig. 5 Cross-sectional SEM micrographs of various Ni(P) layer thickness with Au/Pd/Ni(P) layer contained thin-ENEPIG surface-finished PCB with Sn-58Bi solder joints after aging at 95 °C (Color figure online)

after aging at 105 °C for 1000 h. The Ni_3Sn_4 IMC changed to $(\text{Ni}, \text{Cu})_3\text{Sn}_4$ IMC at the interface of the 0.3 μm Ni(P)–Au/Pd(P)/Ni(P) joint after aging at 105 °C for 1000 h. In contrast, the Ni_3Sn_4 IMCs of the 0.5 μm to 1.0 μm Ni(P)–Au/Pd(P)/Ni(P) joints did not change after aging for up to 1000 h. This was due to the thinner Ni(P) layer thickness of the 0.3 μm Ni(P)–Au/Pd(P)/Ni(P) joint.

Cross-sectional SEM micrographs of the 0.3 μm to 1.0 μm Ni(P)–Au/Pd(P)/Ni(P) joints after aging at 115 °C for 1000 h are shown in Fig. 12. Ni_3Sn_4 (100 h to 300 h) or $(\text{Ni}, \text{Cu})_3\text{Sn}_4$ (500 h to 1000 h) IMCs were formed at the interfaces of the 0.3 μm Ni(P)–Au/

Pd(P)/Ni(P) joints, whereas $(\text{Cu}, \text{Ni})_6\text{Sn}_5$ IMC was dominantly formed at the interface of the 0.3 μm Ni(P)–Au/Pd(P)/Ni(P) joint after aging at 115 °C for 100 h to 1000 h (Fig. 7). Furthermore, the Ni_3Sn_4 IMC was still formed at the interface of the 0.5 μm Ni(P)–Au/Pd(P)/Ni(P) joint after aging at 115 °C for 1000 h, whereas $(\text{Ni}, \text{Cu})_3\text{Sn}_4$ IMC was formed at the interface of the 0.5 μm Ni(P)–Au/Pd(P)/Ni(P) joint after aging at 115 °C for 500 h. These results indicate that the P in the Au/Pd(P)/Ni(P) layer and the Ni(P) layer thickness significantly affects the reaction rate between Au/Pd(Ni(P) and Au/Pd(P)/Ni(P) joints during aging.

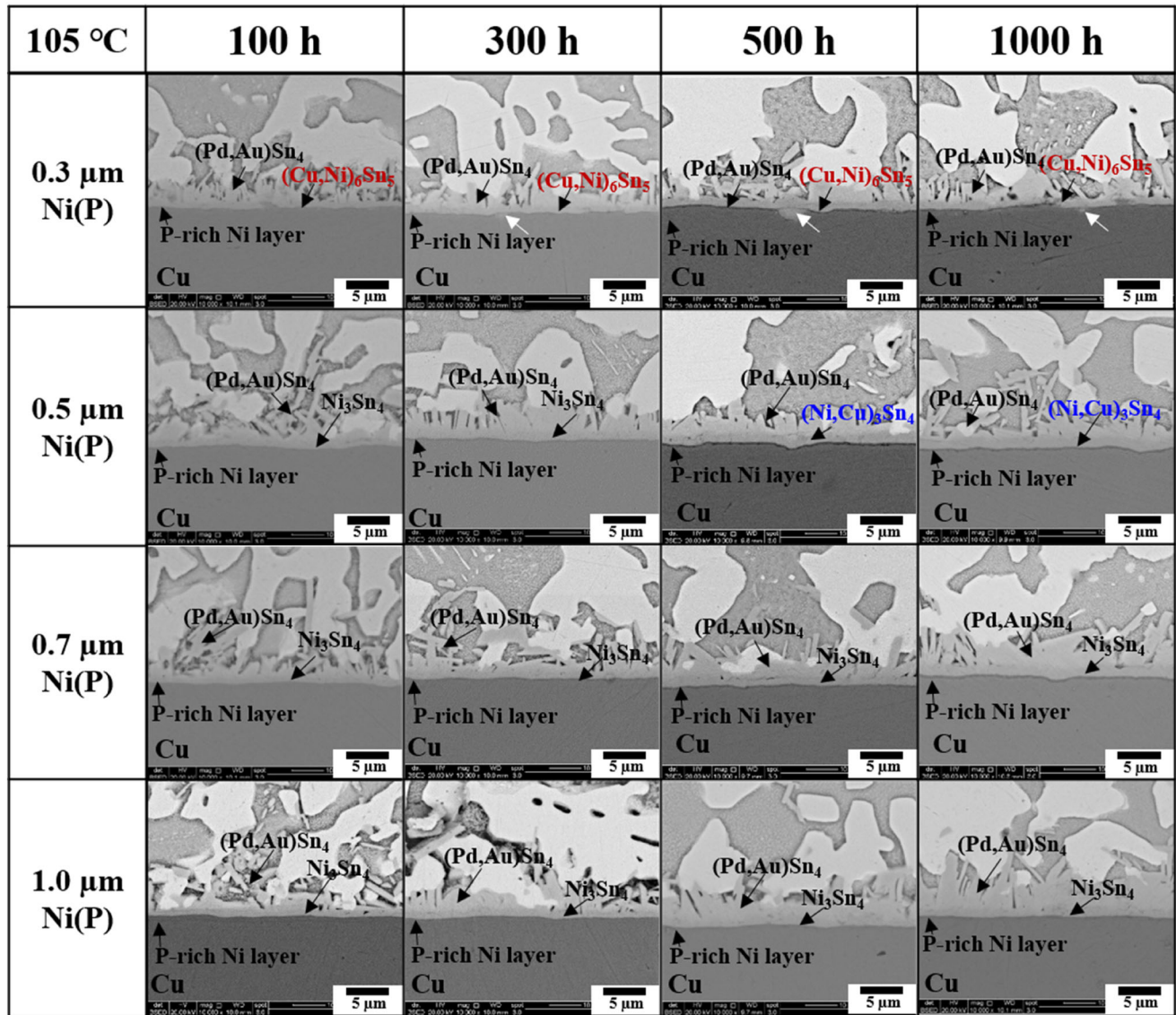


Fig. 6 Cross-sectional SEM micrographs of various Ni(P) layer thickness with Au/Pd/Ni(P) layer contained thin-ENEPIG surface-finished PCB with Sn–58Bi solder joints after aging at 105 °C (Color figure online)

To clarify the differences between the IMC compositions and reaction rates of the Au/Pd/Ni(P) and Au/Pd(P)/Ni(P) joints during aging, EPMA analyses of the 0.3 μm to 0.7 μm Ni(P)–Au/Pd/Ni(P) and Ni(P)–Au/Pd(P)/Ni(P) joints after aging at 115 °C for 1000 h were performed, and the results are shown in Fig. 13. In Fig. 13a, the top- and bottom-side (Cu, Ni)₆Sn₅ IMC layers were formed at the interface between the (Pd, Au)Sn₄ IMC and Cu substrate of the 0.3 μm Ni(P)–Au/Pd/Ni(P) joint after aging at 115 °C for 1000 h. The content of Ni element in the top-side (Cu, Ni)₆Sn₅ IMC was approximately 24.72 at.%, which is a relatively higher content compared to

the bottom-side (Cu, Ni)₆Sn₅ IMC at approximately 8.97 at.% of Ni. In contrast, the content of the Ni element placed with the (Ni, Cu)₃Sn₄ IMC of the 0.3 μm Ni(P)–Au/Pd(P)/Ni(P) joint (Fig. 13b) was approximately 37.26 at.%. In addition, a bottom-side (Ni, Cu)₃Sn₄ IMC beneath the P-rich Ni layer in the Ni(P)–Au/Pd(P)/Ni(P) joint was not observed. This is because the P in the Au/Pd(P)/Ni(P) layer restraint diffusion of Sn in the Sn–Bi solder, and a higher content of Ni remained in the (Ni, Cu)₃Sn₄ IMC of the Au/Pd(P)/Ni(P) joint. For this reason, the Ni content in the Au/Pd(P)/Ni(P) joint was higher than that of the Au/Pd/Ni(P) joint due to same

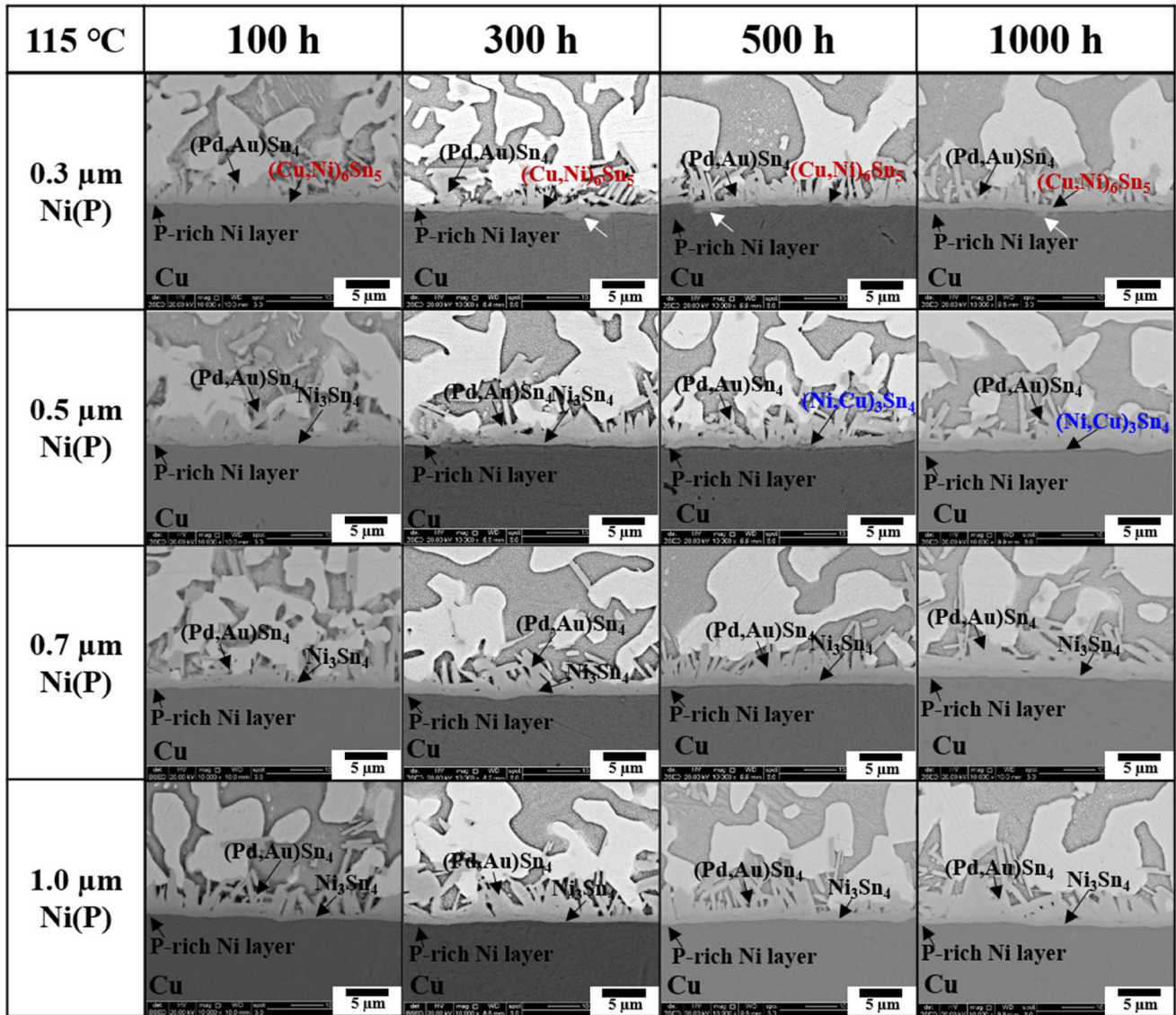


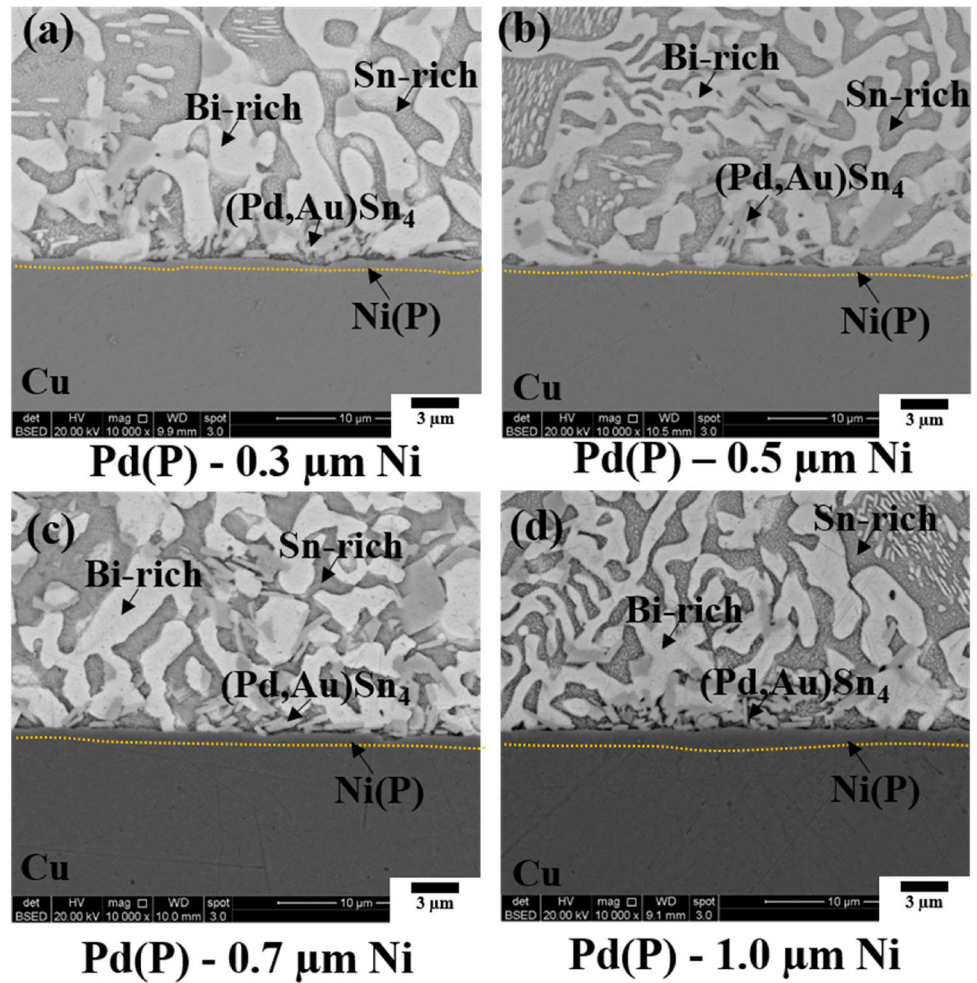
Fig. 7 Cross-sectional SEM micrographs of various Ni(P) layer thickness with Au/Pd/Ni(P) layer contained thin-ENEPIG surface-finished PCB with Sn–58Bi solder joints after aging at 115 °C (Color figure online)

diffusion mechanism of the 0.3 μm Ni(P) layer in the Au/Pd/Ni(P) and Au/Pd(P)/Ni(P) joints. As a result, $(\text{Cu, Ni})_6\text{Sn}_5$ and $(\text{Ni, Cu})_3\text{Sn}_4$ IMCs are formed beneath the $(\text{Pd, Au})\text{Sn}_4$ for the Au/Pd/Ni(P) and Au/Pd(P)/Ni(P) joints, respectively.

The 0.5 μm Ni(P)–Au/Pd/Ni(P) and Pd(P) joints after aging at 115 °C for 1000 h are shown in Fig. 13c and d, respectively. Compared to the 0.3 μm Ni(P)–Au/Pd/Ni(P) and Au/Pd(P)/Ni(P) joints, relatively thick Ni(P) layers are observed. In particular, the Ni element in the Ni(P) layer of the Au/Pd(P)/Ni(P) joint (Fig. 13d) revealed the unreacted remaining Ni(P) layer. A similar tendency was observed in

the thicker Ni(P) layer for the Au/Pd/Ni(P) and Au/Pd(P)/Ni(P) joints, as shown in Fig. 13e, f. These layers had a red color in the Ni mapping results. The unreacted Ni(P) layer in the Au/Pd(P)/Ni(P) joint was thicker than that of the 0.5 μm Ni(P)–Au/Pd/Ni(P) joint, as shown in Fig. 13c and d. Furthermore, the 0.7 μm Ni(P)–Au/Pd/Ni(P) joint also revealed the thicker unreacted Ni(P) layer that was placed below the Ni_3Sn_4 IMC. As a result, the Ni_3Sn_4 IMCs did not change into other IMC phases, and the bottom-side IMCs were not detected at the interfaces of the 0.7 μm to 1.0 μm Ni(P)–Au/Pd/Ni(P) joints and the 0.5 to 1.0 μm Ni(P) layer in the Au/Pd(P)/

Fig. 8 Cross-sectional SEM micrographs of various Ni(P) layer thickness with Au/Pd(P)/Ni(P) layer in thin-ENEPIG surface-finished PCB with Sn–58Bi solder joints after reflow: **a** 0.3 μm Ni(P), **b** 0.5 μm Ni(P), **c** 0.7 μm Ni(P), and **d** 1.0 μm Ni(P) (Color figure online)



Ni(P) joints after aging at 115 °C for 1000 h. As a whole, the consumption rates of the Ni layer for the Au/Pd(P)/Ni(P) joints (Fig. 13b, d, and f) were much slower than those obtained for the Au/Pd/Ni(P) joints (Fig. 13a, c, and e). The remaining Ni(P) layer acted as a good diffusion barrier layer for the Cu from the underlying Cu layer and the Sn from the Sn–Bi solder. Consequently, the underlying Cu layer next to the remaining Ni(P) layer remained intact, as shown in Fig. 13d–f. In contrast, in the thin Ni layer samples, we confirmed the diffusion of Cu into the interfacial IMC phases, as shown in Fig. 13a–c).

Figure 14 shows TEM micrographs and the analysis results of the 0.3 μm Ni(P)–Au/Pd/Ni(P) joint after aging at 115 °C for 1000 h. The (Pd, Au)Sn₄, top- and bottom-side (Cu, Ni)₆Sn₅ IMCs, and P-rich Ni layer were observed at the interface of the joint, as shown in Fig. 13a, b. In Fig. 13b, the destroyed P-rich Ni layer (Area A, bright-gray color) that was placed

between the top- and bottom-side (Cu, Ni)₆Sn₅ IMCs and the non-destroyed P-rich Ni layer (Area B, dark-gray color) were observed in the left-side and right-side of the P-rich Ni layer, respectively. To confirm the Ni and P content in the P-rich Ni layer at the interface of the Au/Pd/Ni(P) joint, mapping results based on TEM micrographs are shown in Fig. 14c. The Ni (blue color) and P (orange color) elements in the right side (Area B) of the P-rich Ni layer indicate a relatively higher content compared to the left side (Area A). In addition, the Sn element (green color) was widely distributed in the Au/Pd/Ni(P) joint as Sn–Bi alloy, (Pd, Au)Sn₄, destroyed P-rich Ni layer, and (Cu, Ni)₆Sn₅ IMCs regions, except for the high content of Ni and P elements distributed in the P-rich Ni layer. Based on these results, it is determined that the Sn in the Sn–Bi alloy and the Cu in the Cu substrate diffused and penetrated part of the P-rich Ni layer. In the line-scan results (Fig. 14d), the Sn (green line) and Cu (red line) elements were mostly

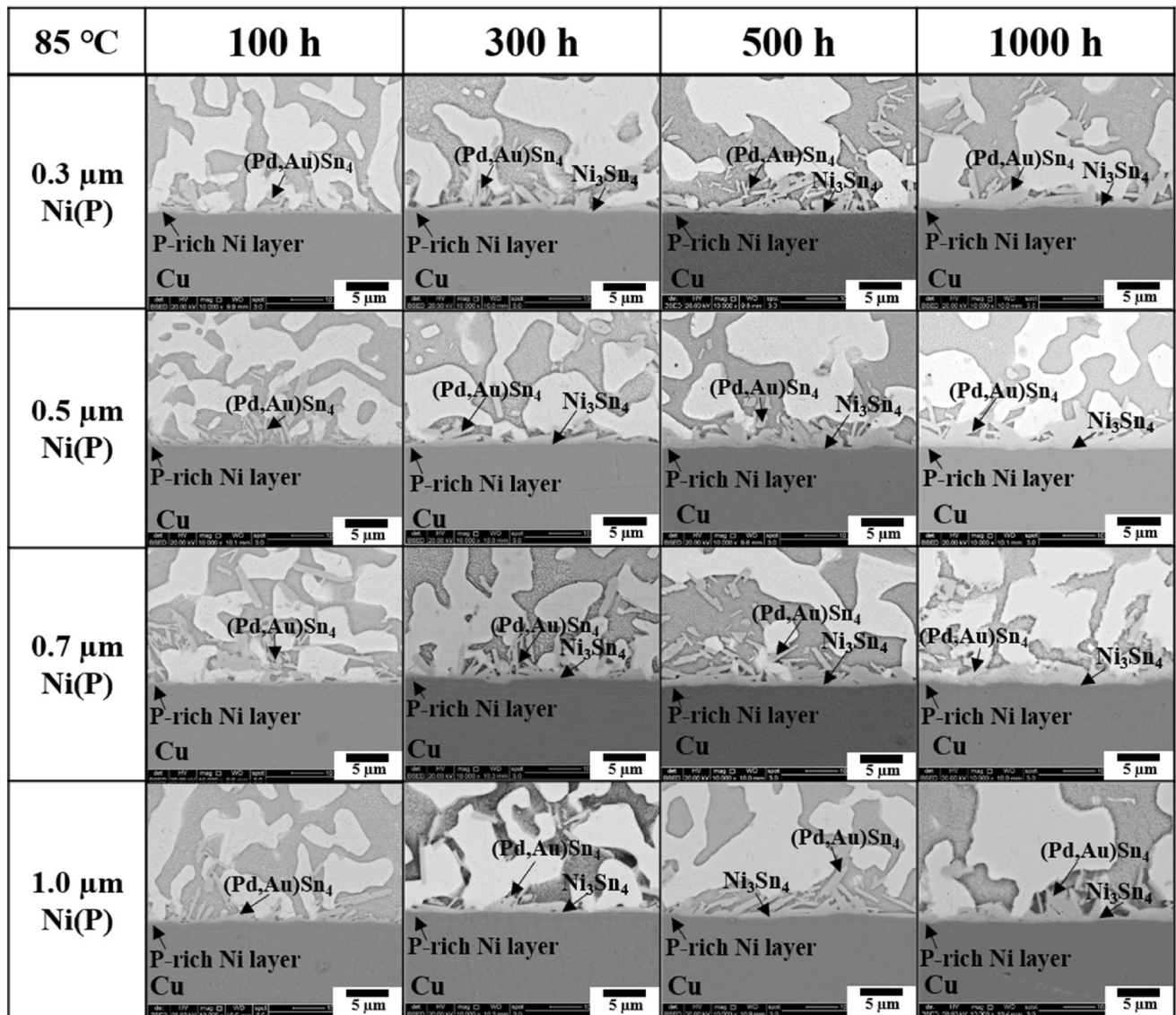


Fig. 9 Cross-sectional SEM micrographs of various Ni(P) layer thickness with Au/Pd(P)/Ni(P) layer contained thin-ENEPIG surface-finished PCB with Sn-58Bi solder joints after aging at 85 °C

distributed in all regions of the detection area from the Cu substrate (left side) to the $(\text{Cu, Ni})_6\text{Sn}_5$ IMC region. Based on these results, it can be inferred that the Ni and P contents of the P-rich Ni layer are reduced due to further diffusion of Sn and Cu. Therefore, the $(\text{Cu, Ni})_6\text{Sn}_5$ IMC was formed at the top- and bottom-side of the interface and in the area of destroyed P-rich Ni layer.

Figure 15 shows TEM micrographs and the analysis results for the 0.3 μm Ni(P)–Au/Pd(P)/Ni(P) joint after aging at 115 °C for 1000 h. Only the top-side $(\text{Ni, Cu})_3\text{Sn}_4$ IMC layer was formed at the interface between $(\text{Pd, Au})\text{Sn}_4$ IMC and the P-rich Ni layer of

the Au/Pd(P)/Ni(P) joint, as shown in Fig. 15a and b. The TEM mapping results are shown in Fig. 15c. In the case of the Au/Pd/Ni(P) joint (Fig. 14c), Sn in the Sn–Bi solder and Cu in the Cu substrate diffused towards the opposite side of each other and destroyed the P-rich Ni layer forming both top- and bottom-side $(\text{Cu, Ni})_6\text{Sn}_5$ IMCs of the Au/Pd/Ni(P) joint after aging at 115 °C for 1000 h. In contrast, the Sn element was almost distributed from the Sn–Bi alloy to $(\text{Pd, Au})\text{Sn}_4$ and the $(\text{Ni, Cu})_3\text{Sn}_4$ IMC region of the Au/Pd(P)/Ni(P) joint, as shown in Fig. 15c. The Ni and P elements were featured continuously horizontal distribution in the P-rich Ni

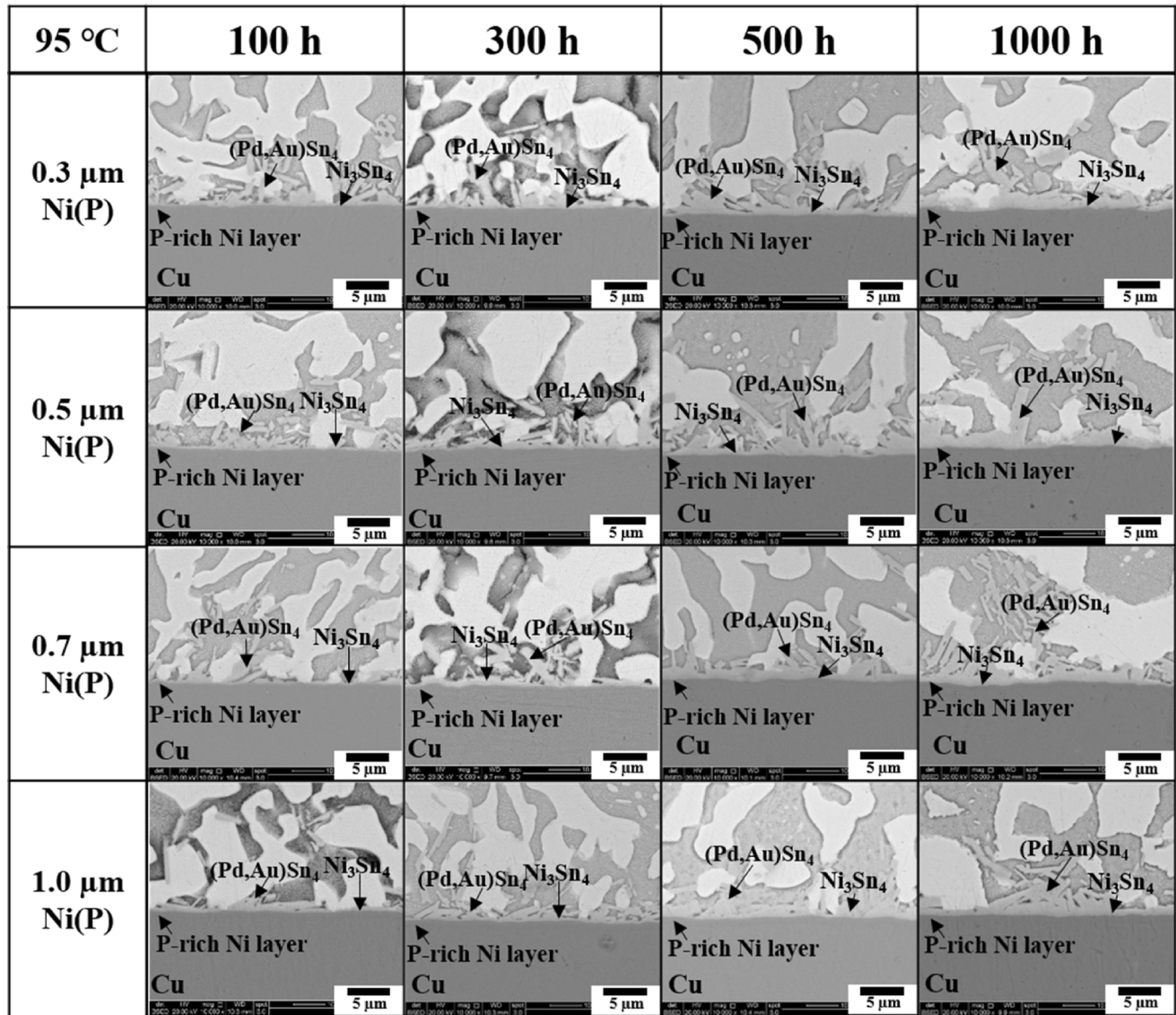


Fig. 10 Cross-sectional SEM micrographs of various Ni(P) layer thickness with Au/Pd(P)/Ni(P) layer contained thin-ENEPIG surface-finished PCB with Sn–58Bi solder joints after aging at 95 °C

layer. These results differ from the Au/Pd/Ni(P) joint, the high contents of P in the Pd layer suppress the reaction rate at the interface. For this reason, the P-rich Ni layer which acts as a diffusion barrier continuously remained at the interface between $(\text{Ni, Cu})_3\text{Sn}_4$ IMC and Cu substrate. These results are based on Ni_3Sn_4 . $(\text{Ni, Cu})_3\text{Sn}_4$ IMC was dominantly formed at the 0.3 μm Ni(P)–Au/Pd(P)/Ni(P) joint and $(\text{Cu, Ni})_6\text{Sn}_5$ IMC was dominantly formed at the Au/Pd(P)/Ni(P) joint during aging. In the line-scan results for the Au/Pd(P)/Ni(P) joint (Fig. 15d), most of the Cu elements (red line) were distributed in the Cu substrate beneath the P-rich Ni

layer, and the Sn element (green line) presents the right side of the P-rich Ni layer (blue-line). In addition, the content of the Ni and P elements in the Au/Pd(P)/Ni(P) joint was higher than those of the Au/Pd/Ni(P) joint. For these reasons, the P in the Au/Pd(P)/Ni(P) joint affects different reaction rate and the high content of Ni and P elements in the P-rich Ni layer plays a role in suppressing the diffusion of Sn in the Sn–Bi solder toward the Cu substrate and Cu in the Cu substrate towards the Sn–Bi solder direction.

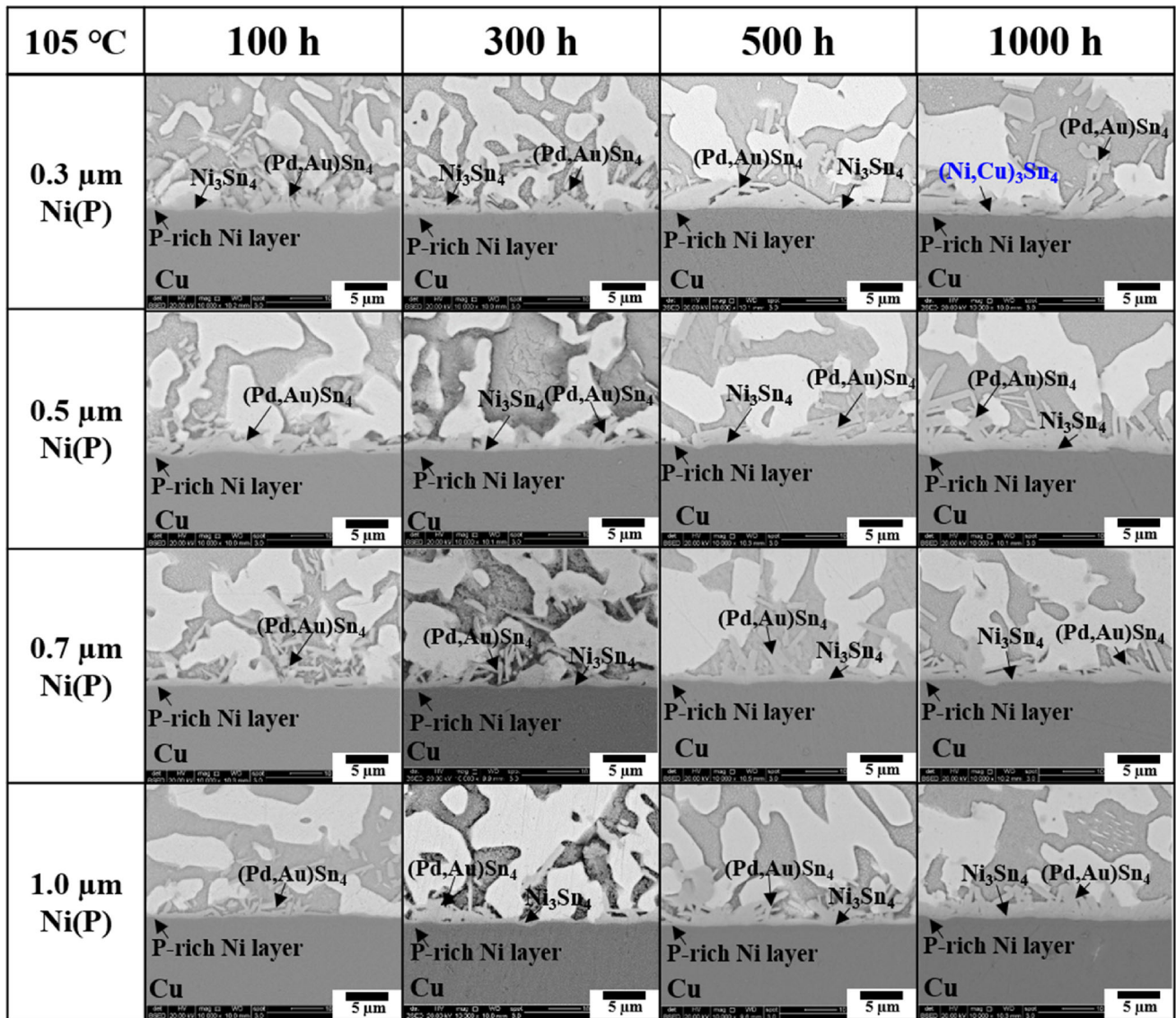


Fig. 11 Cross-sectional SEM micrographs of various Ni(P) layer thickness with Au/Pd(P)/Ni(P) layer contained thin-ENEPIG surface-finished PCB with Sn–58Bi solder joints after aging at 105 °C (Color figure online)

3.2 Mechanical properties during aging

Figure 16 shows the Ni_3Sn_4 IMC thickness of the 0.3 μm to 1.0 μm Ni(P)–Au/Pd/Ni(P) joints after aging treatments. The (Pd, Au) Sn_4 IMC thickness after reflow ranged from 1.6 to 1.8 μm , regardless of the Ni(P) layer thickness of the Au/Pd/Ni(P) joints. A (Cu, Ni) $_6\text{Sn}_5$ IMC layer thickness of 0.3 μm Ni(P)–Au/Pd/Ni(P) joint converged after aging for 300 h at 85 °C to 115 °C (Fig. 16a). In addition, (Ni, Cu) $_3\text{Sn}_4$ IMCs that was formed at the 0.5 μm Ni(P)–Au/Pd/Ni(P) joints converged after aging at 105 °C and 115 °C for 500 h and 1000 h (Fig. 16b). In contrast, the

Ni_3Sn_4 IMC thickness of the 0.7 μm and 1.0 μm Ni(P)–Au/Pd/Ni(P) joints gradually increased with the aging temperature and time, as shown in Fig. 16c and d.

Figure 17 shows the Ni_3Sn_4 IMC thickness of the 0.3 μm to 1.0 μm Ni(P)–Au/Pd(P)/Ni(P) joints after aging treatments. The (Pd, Au) Sn_4 IMC thickness ranged from 1.2 to 1.4 μm . Except for the 0.3 μm Ni(P)–Au/Pd(P)/Ni(P) joints after aging at 105 °C for 1000 h and 115 °C for 500 h, the Ni_3Sn_4 IMC layers were dominantly formed at the interfaces between the (Pd, Au) Sn_4 IMC and P-rich Ni layer. The

interfacial IMC layers gradually increased with an increase in aging temperature and time.

Figure 18 shows the high-speed shear strength of the 0.3 μm to 1.0 μm Ni(P)–Au/Pd/Ni(P) or Au/Pd(P)/Ni(P) joints after aging. The shear strength of these joints is plotted using solid and dashed lines, respectively. High-speed shear strength values of 0.3 μm Ni(P)–Au/Pd/Ni(P) joints rapidly decreased with an increase of the aging time, especially for the high temperatures of 105 °C and 115 °C. Furthermore, the high-speed shear strengths of the 0.3 μm Ni(P)–Au/Pd/Ni(P) joints after aging for 500 h and 1000 h converged at approximately 40 MPa. In

Fig. 13 Elemental mapping results of various Ni(P) layer thickness with (a, c, e) Au/Pd/Ni(P) or (b, d, f) Au/Pd(P)/Ni(P) layer contained thin-ENEPIG surface-finished PCB with Sn–58Bi solder joints after aging at 115 °C for 1000 h: (a, b) 0.3 μm Ni(P), (c, d) 0.5 μm Ni(P), and (e, f) 0.7 μm Ni(P) (Color figure online)

contrast, the high-speed shear strength values of the Au/Pd(P)/Ni(P) joints decreased slightly with each aging condition. The high-speed shear strength of the 0.5 μm Ni(P)–Au/Pd/Ni(P) joints was slightly higher than that of the Au/Pd(P)/Ni(P) joints after aging at 85 °C and 95 °C for 1000 h, as shown in Fig. 18b.

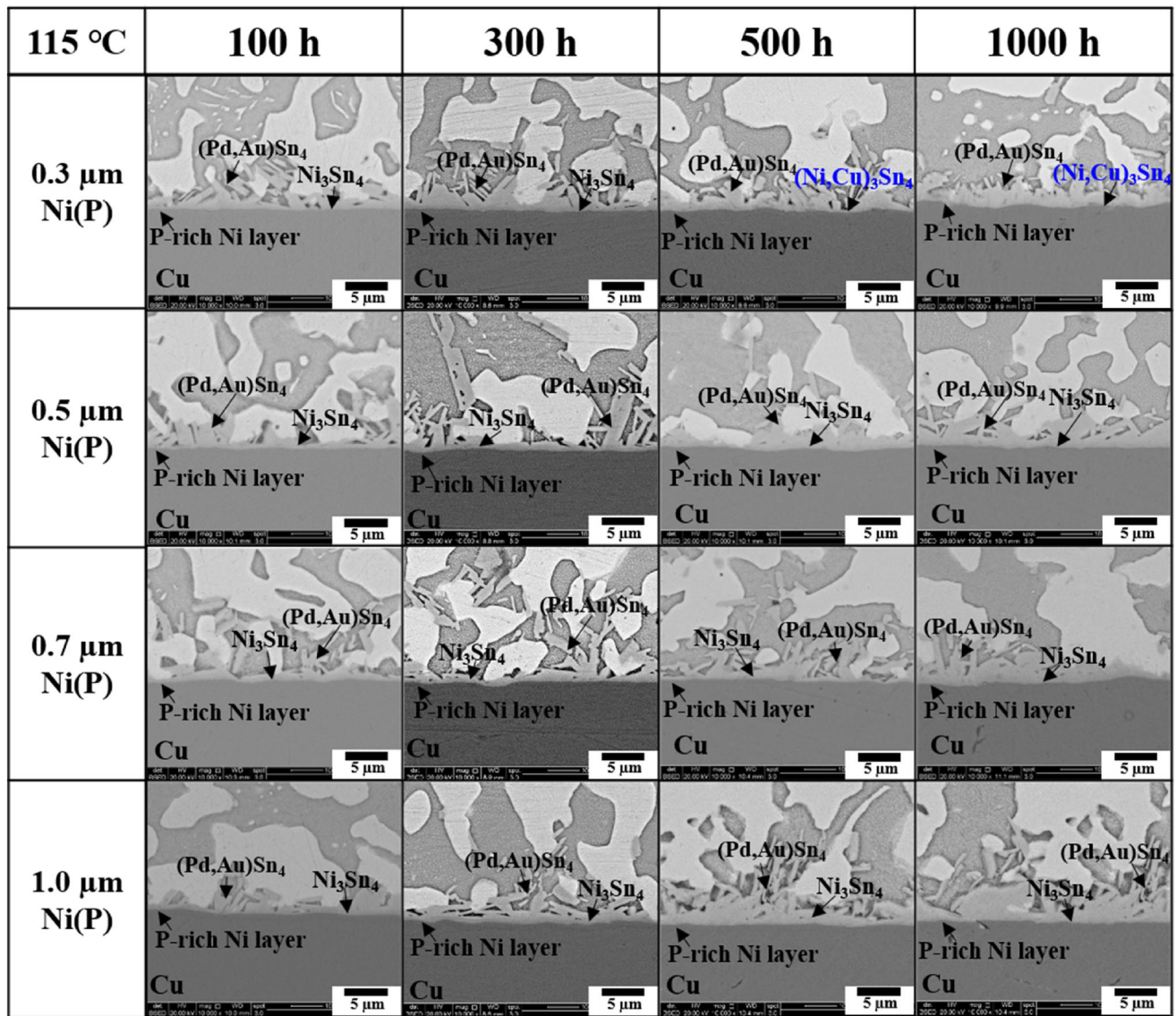
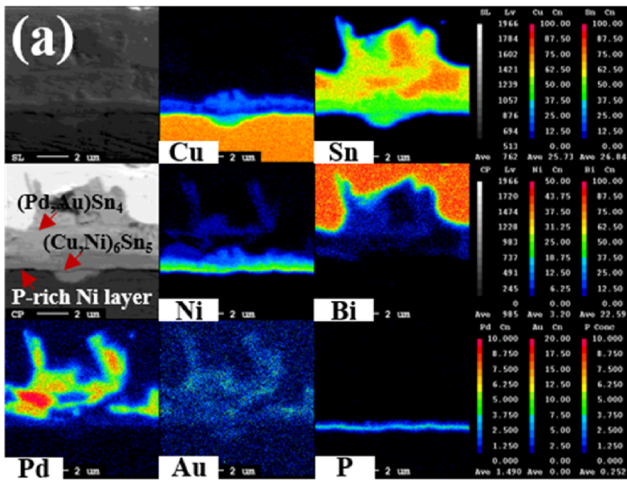
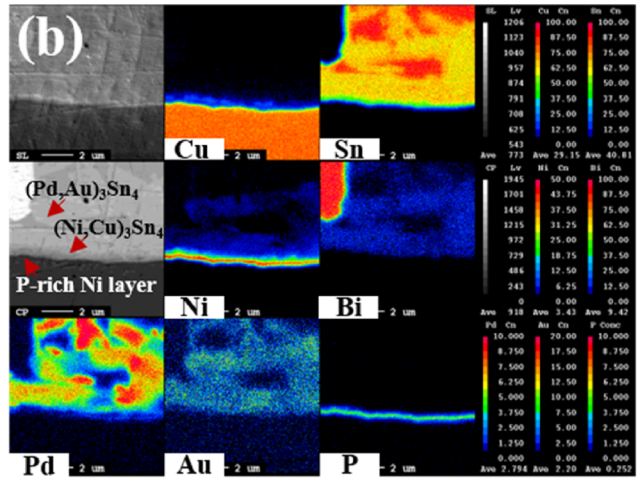


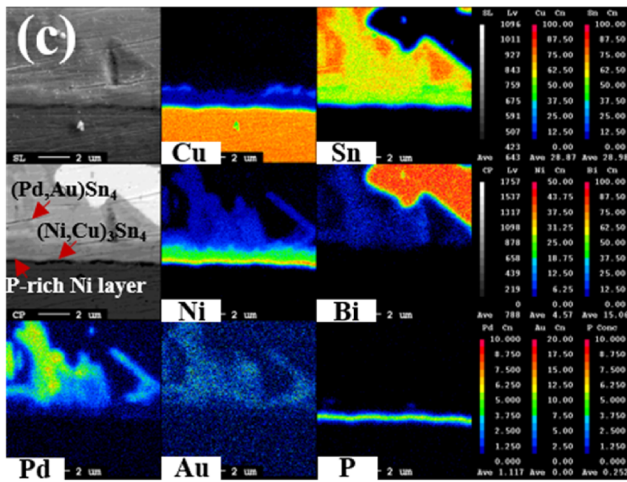
Fig. 12 Cross-sectional SEM micrographs of various Ni(P) layer thickness with Au/Pd(P)/Ni(P) layer contained thin-ENEPIG surface-finished PCB with Sn–58Bi solder joints after aging at 115 °C (Color figure online)



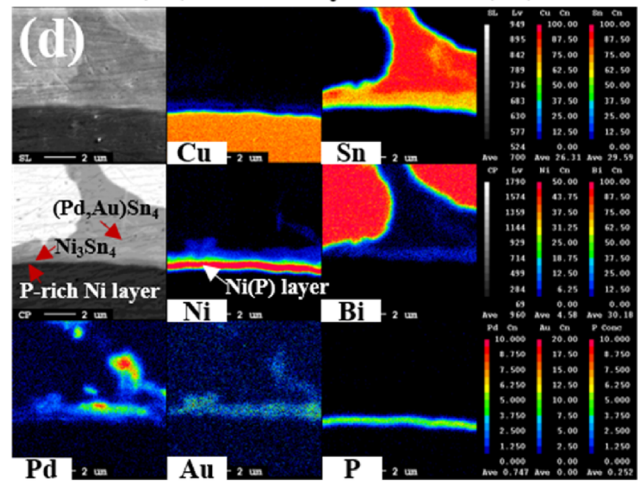
Pure Pd - 0.3 μm Ni(P)



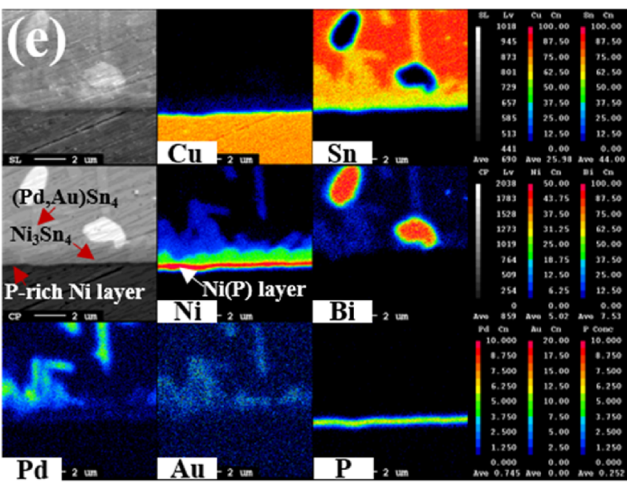
Pd(P) - 0.3 μm Ni(P)



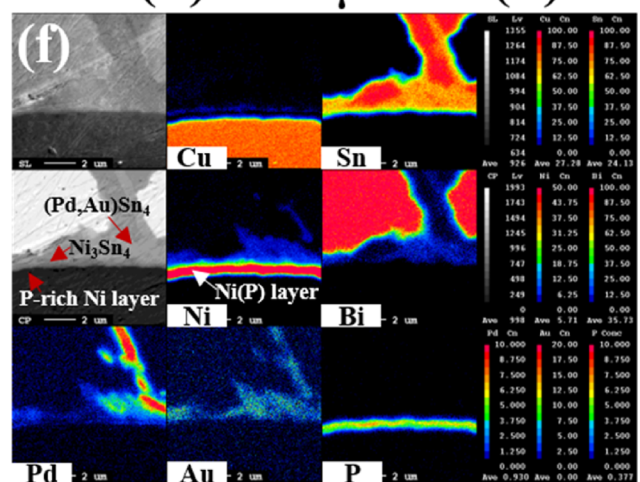
Pure Pd - 0.5 μm Ni(P)



Pd(P) - 0.5 μm Ni(P)

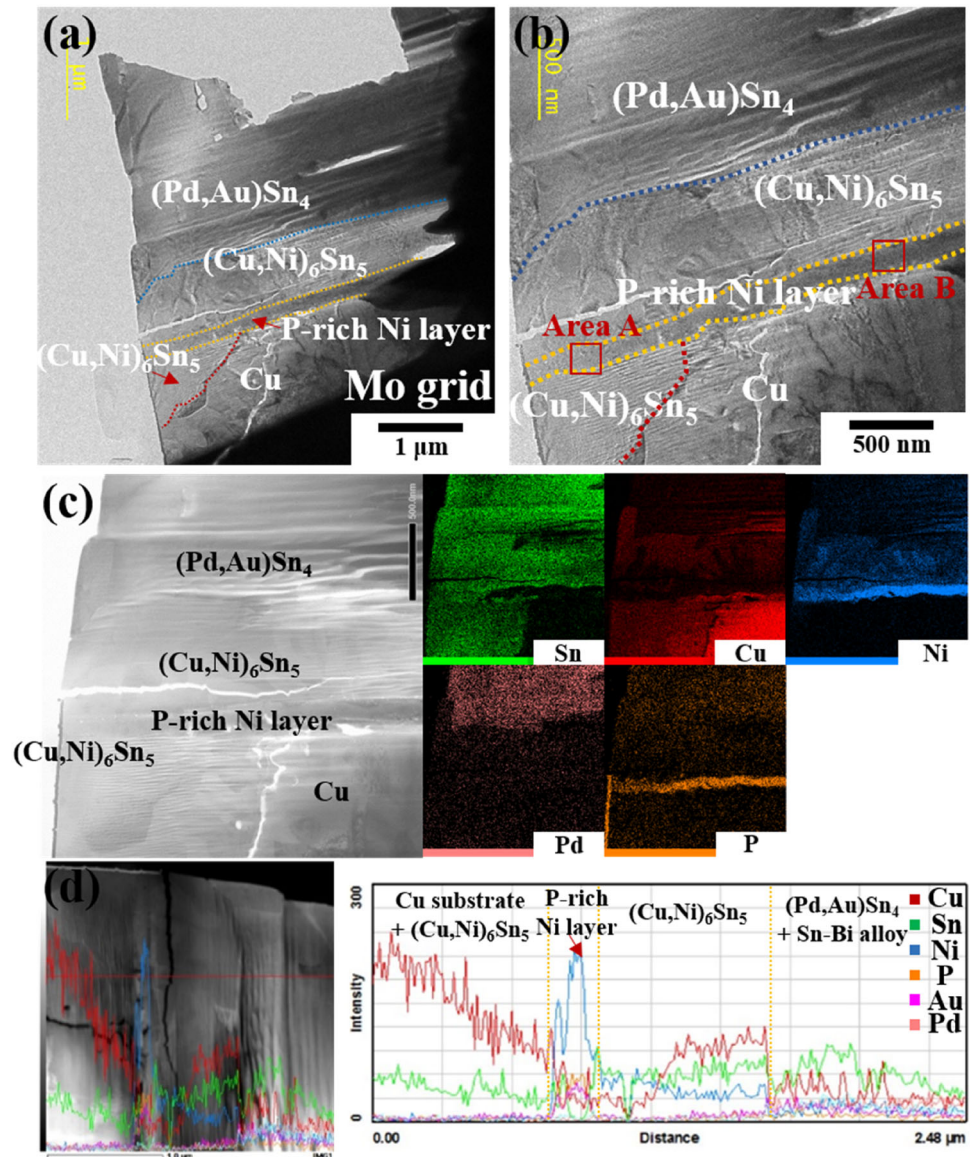


Pure Pd - 0.7 μm Ni(P)



Pd(P) - 0.7 μm Ni(P)

Fig. 14 TEM micrographs and analysis results of 0.3 μm Ni(P) layer thickness with Au/Pd/Ni(P) layer contained thin-ENEPIG surface-finished PCB with Sn–58Bi solder joints after aging at 115 °C for 1000 h: **a** interface of solder joint, **b** high magnified micrograph of (a), **c** mapping results of (a), and **d** line-scan results of (a) (Color figure online)



Otherwise, the high-speed shear strengths of the 0.5 μm Ni(P)–Au/Pd/Ni(P) and Au/Pd(P)/Ni(P) joints after aging at 105 °C and 115 °C had cross-points after aging for 500 h and 1000 h. The high-speed shear strengths of the 0.7 μm and 1.0 μm Ni(P)–Au/Pd/Ni(P) joints have similar values compared to those of the Au/Pd(P)/Ni(P) joints after aging at 85 °C and 95 °C for 1000 h. After aging at 105 °C and 115 °C for 1000 h, the shear strengths of the Au/Pd(P)/Ni(P) joints were slightly lower than those of the Au/Pd/Ni(P) joints. In general, the Sn-based solder joints crucially affect the diffusion behavior leading to the coarsening of microstructures in the solder alloy and the IMCs at the interface under thermal aging. The coarsened microstructure

of the alloy exhibited a lower number of grain boundaries, which can suppress dislocation or crack propagation [32]. In addition, the excessive Cu–Sn IMC has a lower shear strength and faster diffusion rate than the Ni–Sn IMCs at the interface between the substrate and the Sn-based solder alloys under thermal aging. Therefore, the thinner Ni(P) layer in these solder joints led to a reduction in the mechanical strength under thermal aging. As such, the high-speed shear strengths of different Ni(P) layer thickness in the joints results in different reduction rates of the high-speed shear strength and fracture modes, which will be discussed later.

Figure 19 shows the results for the low-speed shear strength of the 0.3 μm to 1.0 μm Ni(P)–Au/Pd/

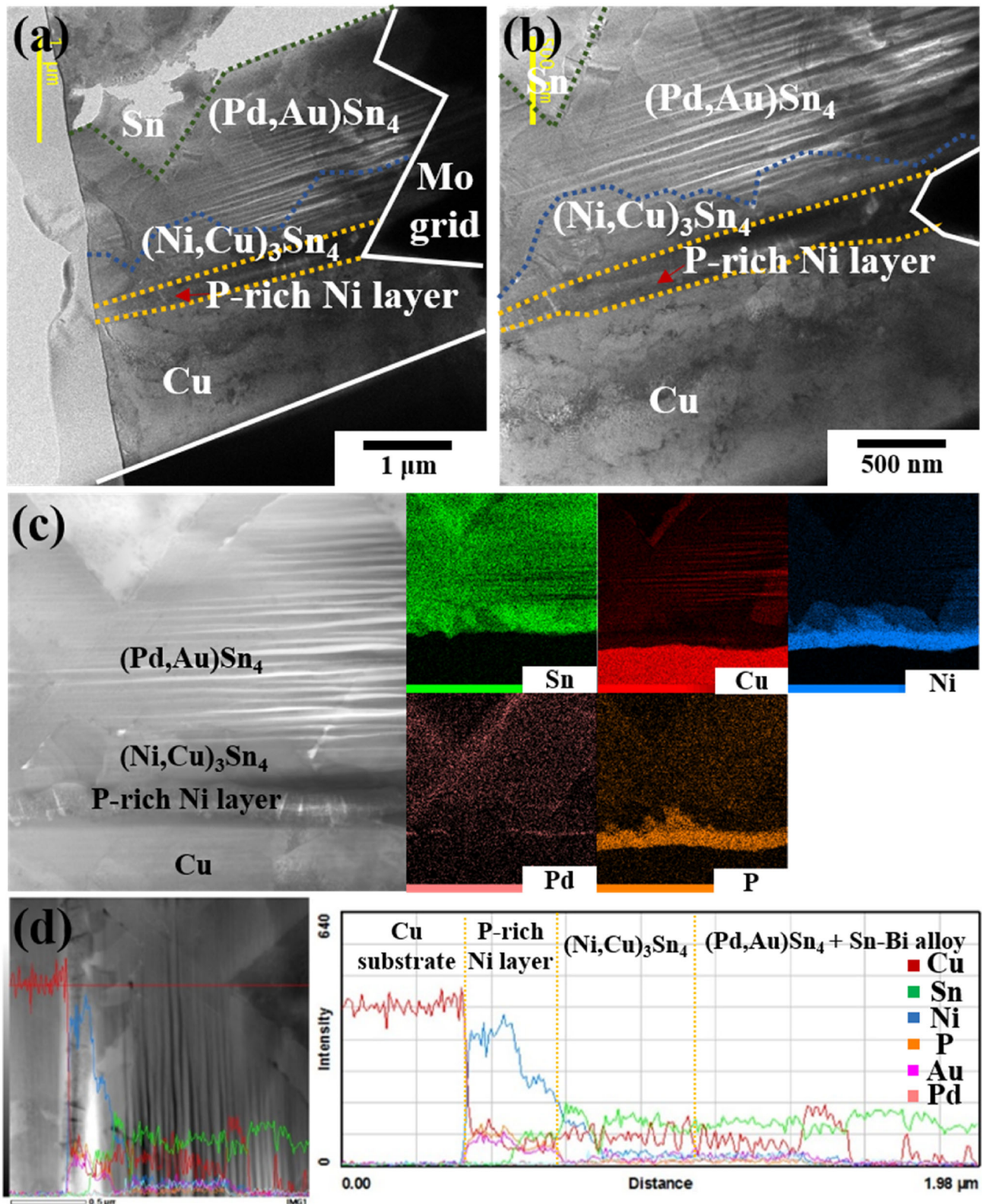


Fig. 15 TEM micrographs and analysis results of 0.3 μm Ni(P) layer thickness with Au/Pd(P)/Ni(P) layer contained thin-ENEPIG surface-finished PCB with Sn–58Bi solder joints after

aging at 115 $^{\circ}\text{C}$ for 1000 h: **a** interface of solder joint, **b** high magnified micrograph of (a), **c** mapping results of (a), and **d** line-scan results of (a) (Color figure online)

Fig. 16 Ni_3Sn_4 IMC thickness of Sn–58Bi solder with various Ni(P) layer with Au/Pd/Ni(P) contained thin-ENEPIG surface-finished PCB joints as functions of aging time and temperature: **a** 0.3 μm Ni(P), **b** 0.5 μm Ni(P), **c** 0.7 μm Ni(P), and **d** 1.0 μm Ni(P) (Color figure online)

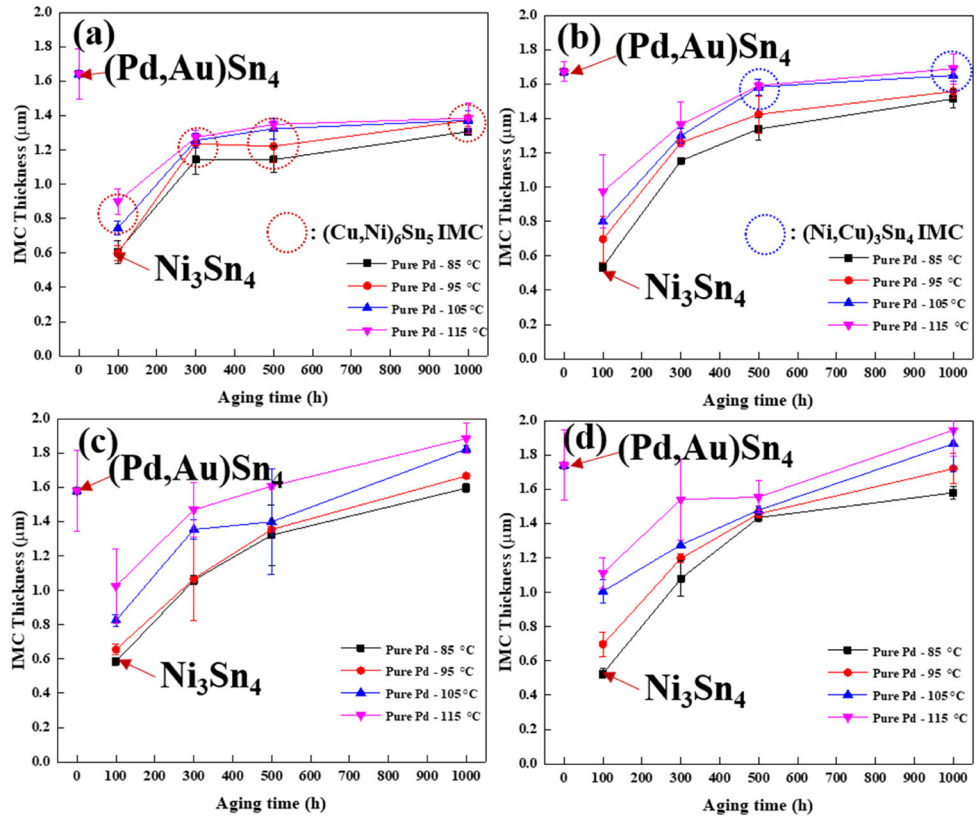


Fig. 17 Ni_3Sn_4 IMC thickness of Sn–58Bi solder with various Ni(P) layer with Au/Pd(P)/Ni(P) contained thin-ENEPIG surface-finished PCB joints as functions of aging time and temperature: **a** 0.3 μm Ni(P), **b** 0.5 μm Ni(P), **c** 0.7 μm Ni(P), and **d** 1.0 μm Ni(P) (Color figure online)

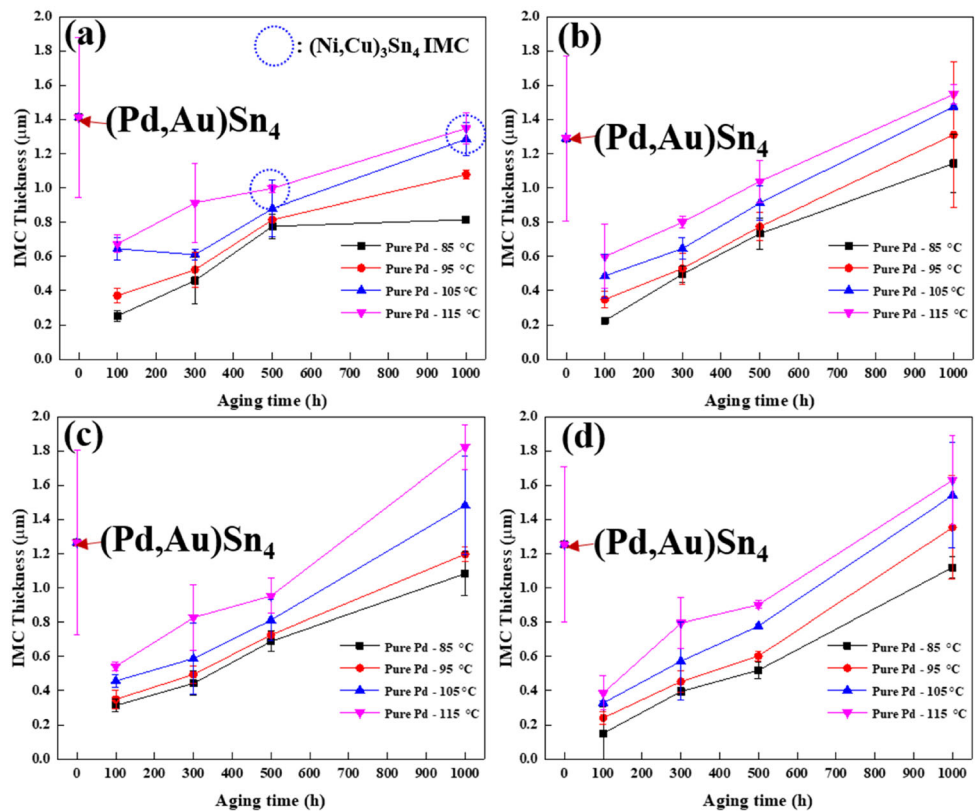
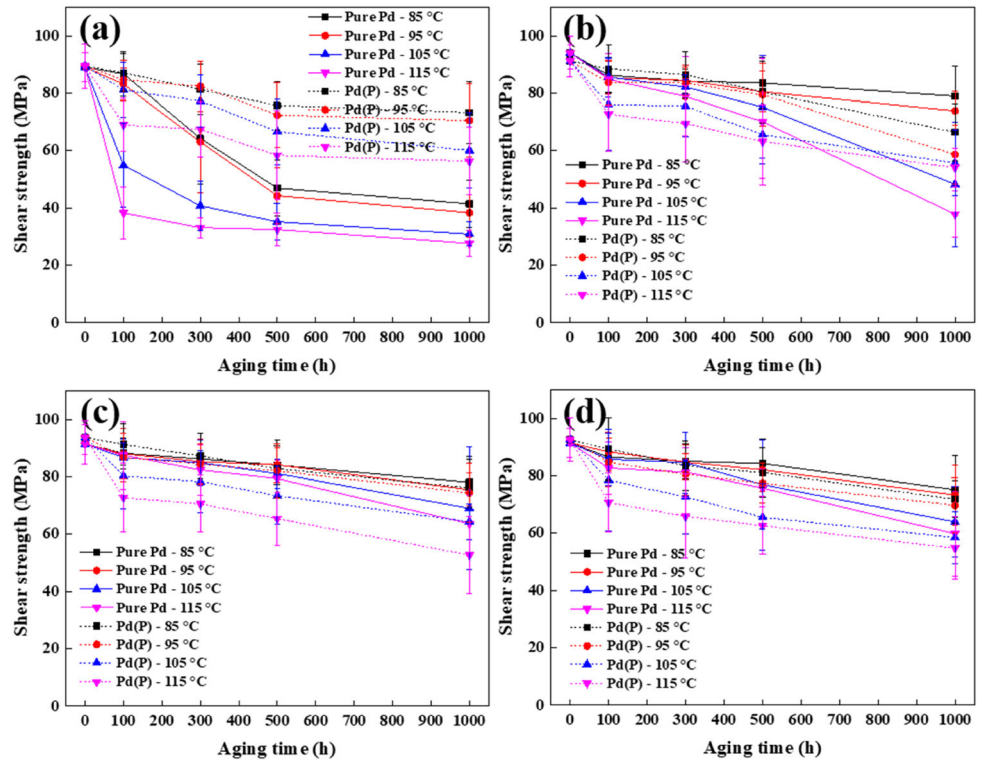


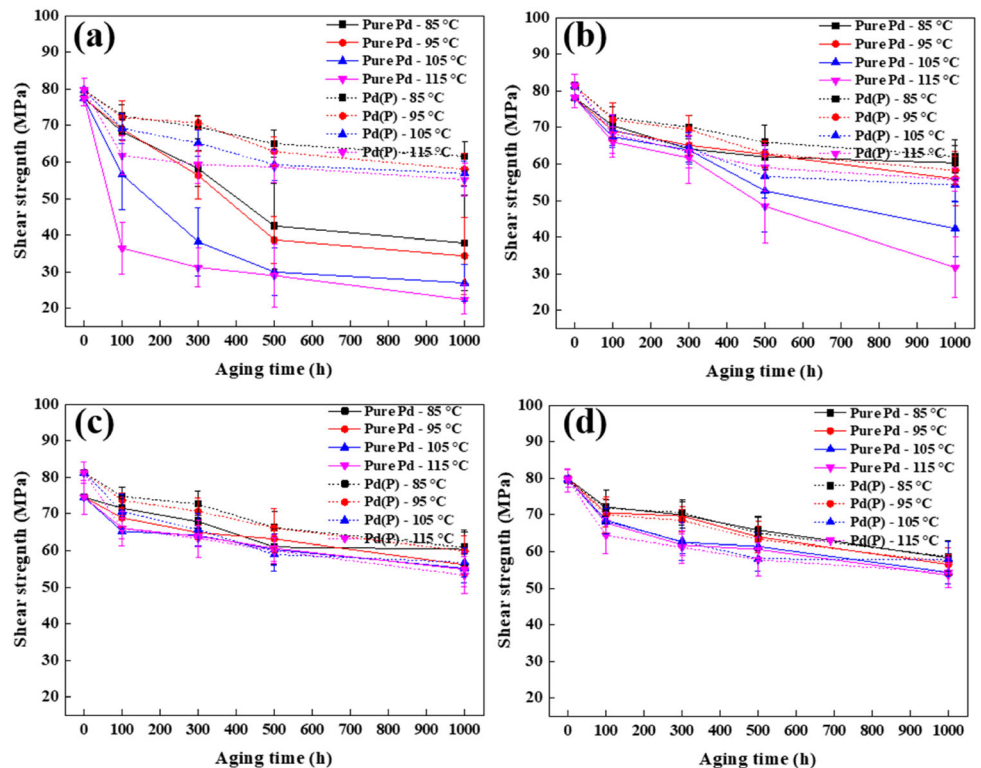
Fig. 18 High-speed shear strength of Sn–58Bi solder with various Ni(P) layer thickness with Au/Pd/Ni(P) or Au/Pd(P)/Ni(P) layer contained thin-ENEPIG surface-finished PCB joints as functions of aging time and temperatures: **a** 0.3 μm Ni(P), **b** 0.5 μm Ni(P), **c** 0.7 μm Ni(P), and **d** 1.0 μm Ni(P) (Color figure online)



Ni(P) or Au/Pd(P)/Ni(P) joints after aging. The low-speed shear strengths of the 0.3 μm Ni(P)–Au/Pd/Ni(P) joints were mostly lower than those of the Au/

Pd(P)/Ni(P) joints, irrespective of the aging temperature and time, as shown in Fig. 19a. The shear strength of the 0.3 μm Ni(P)–Au/Pd/Ni(P) joints

Fig. 19 Low-speed shear strength of Sn–58Bi solder with various Ni(P) layer thickness with Au/Pd/Ni(P) or Au/Pd(P)/Ni(P) layer contained thin-ENEPIG surface-finished PCB joints as functions of aging time and temperatures: **a** 0.3 μm Ni(P), **b** 0.5 μm Ni(P), **c** 0.7 μm Ni(P), and **d** 1.0 μm Ni(P) (Color figure online)



after aging at 105 °C and 115 °C for 1000 h was approximately 30 MPa. For the 0.5 μm-Ni(P) in the Au/Pd/Ni(P) and Au/Pd(P)/Ni(P) joints, the low-speed shear strength of the Au/Pd/Ni(P) joints after aging at 105 °C and 115 °C for 500 h and 1000 h was relatively lower than that of the Au/Pd(P)/Ni(P) joints, as shown in Fig. 19b. However, the low-speed shear strength of the 0.7 μm and 1.0 μm Ni(P)–Au/Pd/Ni(P) and Au/Pd(P)/Ni(P) joints (Fig. 19c and d) has similar shear strength values for the same aging temperatures and times, respectively.

Figure 20 shows fracture surfaces of the 0.3 μm and 1.0 μm Ni(P)–Au/Pd/Ni(P) or Au/Pd(P)/Ni(P) joints after reflows and aging at 115 °C for 1000 h. The fracture surfaces of the 0.3 μm and 1.0 μm Ni(P)–Au/Pd/Ni(P) or Au/Pd(P)/Ni(P) joints after reflow (Fig. 20a, c, e, g) were mostly revealed Sn and Bi elements, determined as ductile fracture modes. The fracture surface of the 0.3 μm Ni(P)–Au/Pd/Ni(P) joint (Fig. 20b) revealed a mostly Cu substrate, whereas the Au/Pd(P)/Ni(P) joint (Fig. 20f) had a (Ni, Cu)₃Sn₄ IMC surface. The fracture modes of the 0.3 μm Ni(P)–Au/Pd/Ni(P) or Au/Pd(P)/Ni(P) joints after aging at 115 °C

for 1000 h were determined to be almost brittle fracture modes. Fracture surfaces of the 1.0 μm Ni(P)–Au/Pd/Ni(P) or Au/Pd(P)/Ni(P) joints were observed for the Ni₃Sn₄ IMC and Sn–Bi solder surfaces and were determined to be mixed fracture modes. However, the fracture modes of both the Au/Pd/Ni(P) and Au/Pd(P)/Ni(P) joints exhibited quite different fracture dimensions, because the Ni₃Sn₄ IMC fracture surface dimension of the Au/Pd(P)/Ni(P) joint was larger than that of the Au/Pd/Ni(P) joint. Therefore, the high-speed shear strength of both the Au/Pd/Ni(P) and Au/Pd(P)/Ni(P) joints exhibited a similar tendency in terms of the brittle fracture rates. The fracture surfaces of the 0.3 μm to 1.0 μm Ni(P)–Au/Pd/Ni(P) or Au/Pd(P)/Ni(P) joints exhibited similar features after low-speed shear tests compared to those of the high-speed shear tests.

To evaluate the effect of the Ni(P) layer thickness on the high-speed shear strength and fracture modes in the Au/Pd/Ni(P) joints, schematic diagrams of the sequential interfacial reactions and fracture behaviors of the Au/Pd/Ni(P) joints are shown in Fig. 21. In the case of the 0.3 μm Ni(P)–Au/Pd/Ni(P) joint after

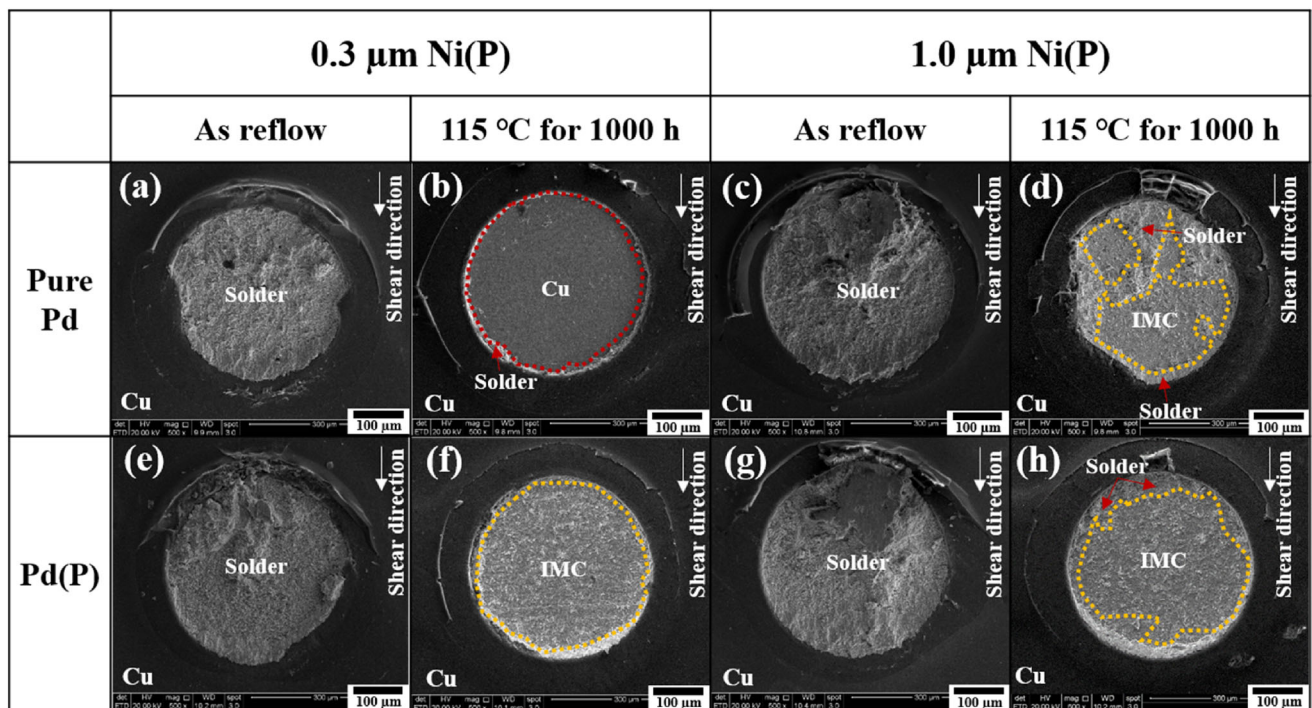


Fig. 20 Fracture surfaces of Sn–58Bi solder joints with (a, b, e, f) 0.3 and (c, d, g, h) 1.0 μm Ni(P) layer thickness with (a–d) Au/Pd/Ni(P) and (e–h) Au/Pd(P)/Ni(P) contained thin-ENEPIG surface-finished PCB as functions of aging time and temperature

after high-speed shear test: a, e after reflow, b, f aged at 115 °C for 1000 h, c, g after reflow, and d, h aged at 115 °C for 1000 h (Color figure online)

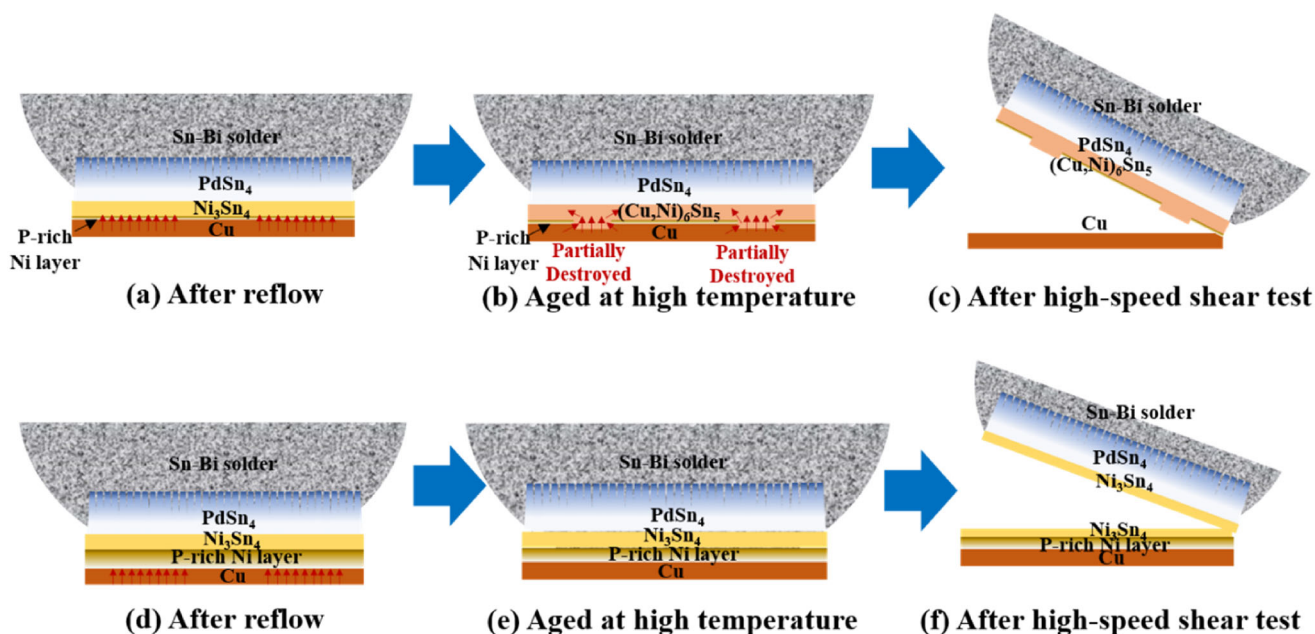


Fig. 21 Schematic diagrams of sequential interfacial reactions and fracture modes of the Sn–58Bi solder with (a–c) 0.3 μm Ni(P) and (d–f) 0.7 to 1.0 μm Ni(P) layer with Au/Pd/Ni(P) layer contained

reflow (Fig. 21a), (Pd, Au)Sn₄ IMC was formed at the interface between the solder and the Ni(P) layer. Then, (Pd, Au)Sn₄ and Ni₃Sn₄ IMCs were formed at the interface during aging. Sequentially, Cu in the Cu substrate diffused towards the Sn–Bi solder direction and changed the IMC composition from Ni₃Sn₄ to (Cu, Ni)₆Sn₅ IMC under aging at high temperatures (Fig. 21b). The Cu and Sn elements penetrated through the P-rich Ni layer during aging, and the P-rich Ni layer was partially destroyed. As a result, fracture occurred at the interface between the bottom-side (Cu, Ni)₆Sn₅ IMC and the partial P-rich Ni layer/Cu substrate of the 0.3 μm Ni(P)–Au/Pd/Ni(P) joint after high-speed shear tests (Fig. 21c). In contrast, in the case of the thick Ni(P) layers, the 0.7 μm and 1.0 μm Ni(P)–Au/Pd/Ni(P) joints formed a relatively thick P-rich Ni layer at the interface between the Ni₃Sn₄ IMC and the Cu substrate. The thick P-rich Ni layer acted as a diffusion barrier for the Sn in the Sn–Bi solder, and the Cu in the Cu substrate during aging. For this reason, the fractures occurred at the interface of the Ni₃Sn₄ IMC layer, as shown in Fig. 21f.

Based on the interfacial reactions and mechanical shear test results obtained in this study, we confirmed that Ni(P)–Au/Pd/Ni(P) or Au/Pd(P)/Ni(P) joints thicker than 0.7 μm with Sn–58Bi solder

in thin-ENEPIG surface-finished PCB joints: a, d after reflow, b, e after aged at high temperature, and c, f after high-speed shear test (Color figure online)

are expected to be high reliability under aging. In addition, the 0.3 μm Ni(P)–Au/Pd(P)/Ni(P) joint has higher reliability compared to the Au/Pd/Ni(P) joint during aging.

4 Conclusions

In this research, the interfacial reactions with microstructure behaviors and the mechanical properties of the 0.3 μm to 1.0 μm Ni(P) layer with a Au/Pd/Ni(P) or Au/Pd(P)/Ni(P) layer in a thin-ENEPIG surface-finished PCB with Sn–58Bi solder joints were investigated at different aging temperatures and times. After reflowing, the (Pd, Au)Sn₄ IMC layer was dominantly formed at the interface of the 0.3 μm to 1.0 μm Ni(P)–Au/Pd/Ni(P) or Au/Pd(P)/Ni(P) joints (initial stage). After aging treatment, the (Cu, Ni)₆Sn₅ IMC was dominantly formed at the interface of 0.3 μm Ni(P)–Au/Pd/Ni(P) joint, whereas the Ni₃Sn₄ IMC was dominantly formed at the interface of 0.3 μm Ni(P)–Au/Pd(P)/Ni(P) joint, except for after aging at 105 $^{\circ}\text{C}$ and 115 $^{\circ}\text{C}$ for 500 h. This is because P and Ni elements in the Au/Pd(P)/Ni(P) and Ni(P) layers that act as a diffusion barrier have a higher content at the Au/Pd(P)/Ni(P) joints than the Au/Pd/Ni(P) joints. In addition, the P in the

Pd layer that was plated on the Ni(P) layer affects the reaction rate and IMC morphology before the Ni in the Ni(P) layer forms Ni–Sn IMCs, and the Ni and P content was relatively high at the interface of the Au/Pd(P)/Ni(P) joint during aging. Except for the 0.5 μm Ni(P) layer in the Au/Pd/Ni(P) joint after aging at 105 $^{\circ}\text{C}$ and 115 $^{\circ}\text{C}$ for 500 h, the Ni_3Sn_4 IMCs were dominantly formed at the interface of the 0.5 μm to 1.0 μm Ni(P)–Au/Pd/Ni(P) and Au/Pd(P)/Ni(P) joints, respectively. This is because thick Ni(P) layers such as 0.7 μm and 1.0 μm have a higher content of Ni and P in the P-rich Ni layer, and unreacted Ni layers during aging.

In the high-speed shear test, the 0.3 μm Ni(P)–Au/Pd(P)/Ni(P) joints has higher shear strength than that of the Au/Pd/Ni(P) joints for each aging conditions. The 0.7 μm and 1.0 μm Ni(P)–Au/Pd/Ni(P) and Au/Pd(P)/Ni(P) joints exhibited a higher shear strength compared to the 0.3 μm and the 0.5 μm Ni(P)–Au/Pd/Ni(P) and Au/Pd(P)/Ni(P) joints. This is because the thick Ni(P) layer suppresses the diffusion of Sn and Cu to form bottom-side (Cu, Ni) $_6\text{Sn}_5$ IMC and destroys the P-rich Ni layer during aging. In the low-speed shear test, the 0.3 μm Ni(P)–Au/Pd(P)/Ni(P) joints had a higher shear strength compared to the Au/Pd/Ni(P) joints under all aging conditions. As results, the high- and low-speed shear strengths of the 0.3 μm Ni(P)–Au/Pd(P)/Ni(P) joints were about a range of 1.5 to 2.3 times higher than those of the 0.3 μm Ni(P)–Au/Pd/Ni(P) joints after aging at 115 $^{\circ}\text{C}$ for 1000 h. In the fracture modes after the high-speed shear test, the 0.3 μm Ni(P)–Au/Pd/Ni(P) joint fractured on the Cu surface while that of the Au/Pd(P)/Ni(P) joint fractured at the IMC surface. The 1.0 μm Ni(P)–Au/Pd/Ni(P) or Au/Pd(P)/Ni(P) joints consisted of mixed (both ductile and brittle) fracture modes. These different shear strength and fracture modes during aging occurred at P in the Au/Pd(P)/Ni(P) layer and these differences affected the different diffusion rate at the interface including the destroyed P-rich Ni layer, and formed the bottom-side (Cu, Ni) $_6\text{Sn}_5$ IMC. Therefore, the 0.7 μm and 1.0 μm Ni(P) layers with both Au/Pd/Ni(P) and Au/Pd(P)/Ni(P) joints with Sn–58Bi solder are expected to exhibit long-term reliability during aging.

References

1. T.K. Lee, H. Ma, K.C. Liu, J. Xue, J. Electron. Mater. **39**, 2564 (2010). <https://doi.org/10.1007/s11664-010-1352-8>
2. Y. Oda, N. Fukumuro, S. Yae, J. Electron. Mater. **47**, 2507 (2018). <https://doi.org/10.1007/s11664-018-6067-2>
3. Y.W. Yen, P.H. Tsai, Y.K. Fang, S.C. Lo, Y.P. Hsieh, C. Lee, J. Alloys Compd. **503**, 25 (2010). <https://doi.org/10.1016/j.jallcom.2010.04.241>
4. C.Y. Ho, J.G. Duh, C.W. Lin, C.J. Lin, Y.H. Wu, H.C. Hong, T.H. Wang, J. Mater. Sci. **48**, 2724 (2013). <https://doi.org/10.1007/s10853-012-7070-2>
5. T. You, Y. Kim, W. Jung, J. Moon, H. Choe, J. Alloys Compd. **486**, 242 (2009). <https://doi.org/10.1016/j.jallcom.2009.07.085>
6. H.W. Miao, J.G. Duh, Mater. Chem. Phys. **71**, 255 (2001). [https://doi.org/10.1016/S0254-0584\(01\)00298-X](https://doi.org/10.1016/S0254-0584(01)00298-X)
7. A.K. Gain, T. Fouzder, Y.C. Chan, W.K.C. Yung, J. Alloys Compd. **509**, 3319 (2011). <https://doi.org/10.1016/j.jallcom.2010.12.048>
8. M.N. Islam, Y.C. Chan, Mater. Sci. Eng. B **117**, 246 (2005). <https://doi.org/10.1016/j.mseb.2004.11.027>
9. B.F. Dyson, T.R. Anthony, D. Turnbull, Appl. Phys. Lett. **38**, 3408 (1967). <https://doi.org/10.1063/1.1710127>
10. J.W. Yoon, S.B. Jung, J. Alloys Compd. **448**, 177 (2008). <https://doi.org/10.1016/j.jallcom.2006.10.052>
11. C.M. Tsai, W.C. Luo, C.W. Chang, Y.C. Shieh, C.R. Kao, J. Electron. Mater. **33**, 1424 (2004). <https://doi.org/10.1007/s11664-004-0082-1>
12. J.W. Yoon, S.B. Jung, J. Alloys Compd. **458**, 200 (2008). <https://doi.org/10.1016/j.jallcom.2007.04.014>
13. Y.L. Lin, Y.S. Lai, C.M. Tsai, C.R. Kao, J. Electron. Mater. **35**, 2147 (2006). <https://doi.org/10.1007/s11664-006-0325-4>
14. P. Liu, P. Yao, J. Liu, J. Alloys Compd. **470**, 188 (2009). <https://doi.org/10.1016/j.jallcom.2008.02.102>
15. L.C. Tsao, M.W. Wu, S.Y. Chang, J. Mater. Sci: Mater. Electron. **23**, 681 (2012). <https://doi.org/10.1007/s10854-011-0471-1>
16. C.F. Tseng, J.G. Duh, Mater. Sci. Eng. A **580**, 169 (2013). <https://doi.org/10.1016/j.msea.2013.05.058>
17. C.M. Liu, C.E. Ho, W.T. Chen, C.R. Kao, J. Electron. Mater. **30**, 1152 (2001). <https://doi.org/10.1007/s11664-001-0143-7>
18. W.C. Luo, C.E. Ho, J.Y. Tsai, Y.L. Lin, C.R. Kao, Mater. Sci. Eng. A **396**, 385 (2005). <https://doi.org/10.1016/j.msea.2005.02.008>
19. C.Y. Ho, J.G. Duh, Mater. Sci. Eng. A **611**, 162 (2014). <https://doi.org/10.1016/j.msea.2014.05.049>
20. W.H. Wu, C.S. Lin, S.H. Huang, C.E. Ho, J. Electron. Mater. **39**, 2387 (2010). <https://doi.org/10.1007/s11664-010-1351-9>

21. B.M. Chung, Y.H. Baek, J. Choi, J.Y. Huh, *J. Electron. Mater.* **41**, 3348 (2012). <https://doi.org/10.1007/s11664-012-2320-2>
22. K.P.L. Pun, M.N. Islam, J. Rotanson, C.W. Cheung, A.H.S. Chan, *J. Electron. Mater.* **47**, 5191 (2018). <https://doi.org/10.1007/s11664-018-6385-4>
23. Z. Liu, J. Cai, Q. Wang, X. He, Y. Chen, *J. Electron. Mater.* **43**, 3341 (2014). <https://doi.org/10.1007/s11664-014-3236-9>
24. J.W. Yoon, B.I. Noh, S.B. Jung, *J. Electron. Mater.* **40**, 1950 (2011). <https://doi.org/10.1007/s11664-011-1686-x>
25. Y.M. Kim, J.Y. Park, Y.H. Kim, *J. Electron. Mater.* **41**, 763 (2012). <https://doi.org/10.1007/s11664-012-1921-0>
26. C.E. Ho, L.H. Hsu, C.H. Yang, T.C. Yeh, P.T. Lee, *Thin Solid Films* **584**, 257 (2015). <https://doi.org/10.1016/j.tsf.2014.12.026>
27. T.T. Chou, C.J. Fleshman, H. Chen, J.G. Duh, *J. Mater. Sci: Mater. Electron.* **30**, 2342 (2019). <https://doi.org/10.1007/s10854-018-0507-x>
28. J.W. Yoon, J.H. Back, S.B. Jung, *Surf. Interface Anal.* **50**, 1046 (2018). <https://doi.org/10.1002/sia.6419>
29. J. Keller, D. Baither, U. Wilke, G. Schmitz, *Acta Mater.* **59**, 2731 (2011). <https://doi.org/10.1016/j.actamat.2011.01.012>
30. J.H.L. Pang, T.H. Low, B.S. Xiong, X. Luhua, C.C. Neo, *Thin Solid Films* **462–463**, 370 (2004). <https://doi.org/10.1016/j.tsf.2004.05.092>
31. J. Kim, S.B. Jung, J.W. Yoon, *J. Alloys Compd.* **820**, 153396 (2020). <https://doi.org/10.1016/j.jallcom.2019.153396>
32. M. Aamir, R. Muhammad, N. Ahmed, M. Waqas, *Microelectron. Reliab.* **78**, 311 (2017). <https://doi.org/10.1016/j.microrel.2017.09.022>

Publisher's Note Springer Nature remains neutral with regard to jurisdictional claims in published maps and institutional affiliations.